CHALMERS

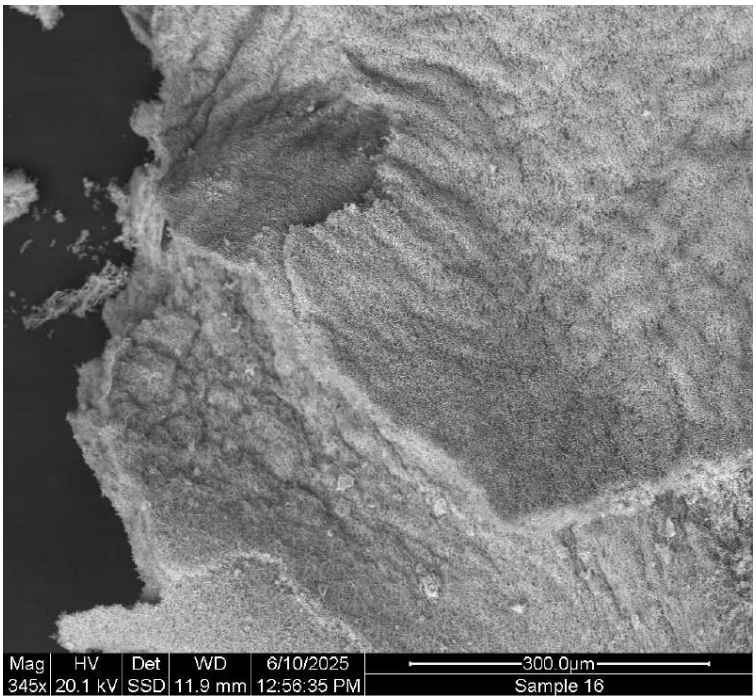

Synthesis and performance assessment of nanofibrous oxygen carriers in chemical looping dry reforming of methane

- Comparing the effects of dopant metals in iron based oxygen carriers

Master's thesis in chemical engineering

ERIK SANDELL

Department of Chemistry and Chemical Engineering
CHALMERS UNIVERSITY OF TECHNOLOGY
Gothenburg 2025
www.chalmers.se

Master's Thesis 2025

Synthesis and performance assessment of nanofibrous oxygen carriers in chemical looping dry reforming of methane

- Comparing the effects of dopant metals in iron based oxygen carriers

ERIK SANDELL

CHALMERS

Department of Chemistry and Chemical Engineering
Chalmers University of Technology
Gothenburg 2025

Synthesis and performance assessment of nanofibrous oxygen carriers in chemical looping dry reforming of methane
- Comparing the effects of dopant metals in iron based oxygen carriers
ERIK SANDELL

Supervisor: Professor Ramsagar Vooradi
Examiner: Professor Henrik Leion

Master's Thesis 2025
Department of Chemistry and Chemical Engineering
Chalmers University of Technology
SE-412 58 Gothenburg
Telephone +46 31 772 1000

Cover art: SEM image of nanofibrous oxygen carrier material, Erik Sandell

Written in LaTeX
Gothenburg 2025

Synthesis and performance assessment of nanofibrous oxygen carriers in chemical looping dry reforming of methane

ERIK SANDELL
Department of Chemistry and Chemical Engineering
Chalmers University of Technology

Abstract

Chemical looping technology is an interesting method of utilizing carbonaceous fuels while alleviating some of the environmental impacts of its usage. It has been previously implemented in combustion processes and further research is being conducted to investigate its potential in other processes such as methane reformation. For chemical looping technology to be viable in this application there is a need for efficient oxygen carrying materials. This thesis aimed to synthesize and test an oxygen carrying material with a nanofibrous structure which could be used in dry methane reformation applications. Using electrospinning, a substrate of was synthesized on which metals could be impregnated resulting in a nanofibrous material with metal oxides bound to an alumina fibrous substrate. The metals investigated in this project was iron, cerium, manganese, strontium and nickel. These materials were chosen due to their relative abundance and iron was the main metal constituent of the materials, while the other metals was used as dopants. The resulting materials were used in methane reformation successfully, with iron-nickel and iron-Strontium being the most effective of the materials investigated.

Keywords: Nanofibrous oxygen carrier, Chemical looping, Dry reformation of methane,

0.1 Foreword

This study was carried out as a joint project between NIT Warangal, India, and Chalmers University, Sweden. The first half of the project focused on material preparation and was done in India, and the second half which focused on material testing was done in Sweden. During my stay in India I had the pleasure of meeting many wonderful people and was lucky to be invited on trips to several local attractions.

I would like to thank my examiner Prof. Henrik Leion for offering me the great opportunity to carry out this project. I would also like to thank my supervisor Prof. Ramsagar Vooradi and Prof. Venkata Suresh for their guidance and great hospitality. Finally, I would like to thank my fellow researchers Raju Payyavula, Hemanth Rajesh and Vikas Sharma for their hospitality and helping me during my visit in India.

Erik Sandell, Gothenburg, June 2025

Acronyms

Alac	Aluminium acetyl acetonate
AR	Air Reactor
CDR	Carbon Dioxide Removal
CH_4	Methane
CLC	Chemical Looping Combustion
CLR	Chemical Looping Reformation
CLT	Chemical Looping Technology
CO	Carbon monoxide
CO_2	Carbon dioxide
DRM	Dry Reformation of Methane
DMF	Dimethylformamide
EDS	Electron Dispersion X-ray Spectroscopy
FR	Fuel Reactor
H_2	Hydrogen gas
N.B.	Nota Bene (note well)
OC	Oxygen carrier(s)
PAN	Polyacrylonitrile
SMR	Steam Methane Reformation
SEM	Scanning Electron Microscope
Syngas	Synthetis gas
DMF	Dimethylformamide

Contents

1

Introduction

1.1 Background

Increasing levels of carbon dioxide (CO_2) in the atmosphere is a side effect of the extensive use of carbonaceous fuels in society [1]. These emissions lead to several global issues, of which climate change is one of the most pressing concerns in society [2]. According to the United nations environment programme, 68% of the current greenhouse gas emissions comes from fossil fuels in the form of CO_2. Although there is ongoing development of renewable energy sources to reduce CO_2 emissions, it is very likely that carbonaceous fuels (fossil or otherwise) will remain a means of energy production in the foreseeable future [1]. A possible method of limiting the impact of carbonaceous fuel usage is carbon dioxide removal (CDR), in which CO_2 is removed from the atmosphere and sequestered in reservoirs or solid material [1]. CDR is most viable when capturing CO_2 at the emission sources because of the higher CO_2 concentration in the exhaust gas streams compared to the general atmosphere, but this method is quite expensive and not very efficient due to the dilution of CO_2 in the exhaust gases leading to costly separation processes [3] [4]. To alleviate this problem, new methods have been developed to separate atmospheric oxygen from superfluous gases such as nitrogen. The pure oxygen can then be used for combustion of carbonaceous fuels and the resulting exhaust gas will mainly contain CO_2 and water, which can be separated quite easily through condensation[3] [5]. Removing nitrogen in the gas intake will also prevent other greenhouse gases, such as nitrogen oxides from forming [4].

One adaptation of oxygen separation in the conversion of fuels is Chemical looping technologies (CLT), which utilizes oxygen carrier (OC) material to absorb oxygen from air and later releasing the bound oxygen for reactions to take place. The OC material is generally made up of metal oxides and the reaction steps take place in two separate reactors with the OC circulating between the two reactors. The type of metal can vary depending on the process, and the OC material can consist of a tailored material or simply crushed metal ore. A simplified CLT layout is shown in figure 1.1, where the OC absorbs oxygen in an air reactor (AR) and releases the oxygen in a fuel reactor (FR).

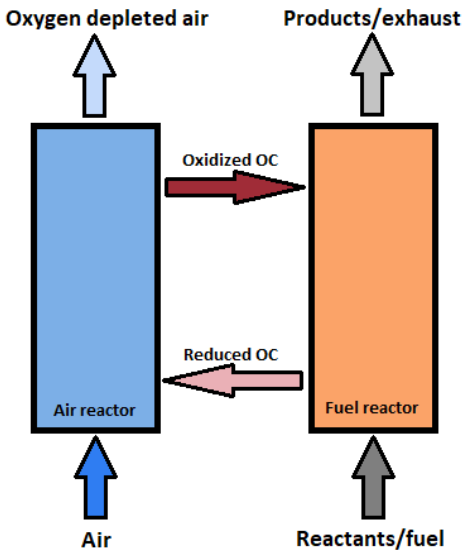

Figure 1.1: Simplified layout of a CLT system. The oxygen carrier absorbs oxygen from the air in the air reactor and releases it in the fuel reactor

So far, CLT has successfully been applied in chemical looping combustion (CLC) and the method also shows potential to be used in a process called chemical looping reforming (CLR) [4] in which fuel is partially oxidized into a mixture of carbon monoxide (CO) and hydrogen (H_2) called synthetis gas (syngas)[6].
The conventional methods of syngas production are steam methane reformation (SMR) and dry reformation of methane (DRM) and they are extensively used to produce hydrogen [7]. SMR uses heat, methane (CH_4) and steam to produce H_2, CO and CO_2 in varying ratios depending on the processing method, as the methane can be pertially or fully oxidized according to equations 1.1 and 1.2.

$$CH_4 + H_2O => 3H_2 + CO \tag{1.1}$$

$$CH_4 + 2H_2O => 4H_2 + CO_2 \tag{1.2}$$

DRM instead uses heat and CO_2 to partially oxidize the CH_4 into CO and H_2 in a reaction shown in equation 1.3. Dry reformation of CH_4 is particularly interesting as CH_4 and CO_2 (two greenhouse gases) are used to produce useful syngas, and it serves as a way to utilizing the very stable CH_4 for downstream production of useful chemicals. It also produces CO and H_2 in a 1:1 ratio which is better suited for some downstream uses than the higher CO:H_2 ratios of the SMR method [8].

$$CH_4 + CO_2 => 2H_2 + 2CO \tag{1.3}$$

Both SMR and DRM methods can be improved by the use of catalysts, which often use nickel [7], a common issue is the formation of carbon deposits on the catalyst surface which deactivates the catalyst, and sintering of the catalyst material which reduces its catalytic activity [7].
CLR has become a very active research topic as an alternative to the conventional methods. The chemical reactions in the chemical looping-DRM process are shown in equation 1.4 where methane reacts with the OC. The OC is then reoxidized with

CO_2 as shown in equation 1.5 Oxygen carriers are denoted as MO in the equation, as they are usually metal oxides. The choice of metal depends on the process the OC is to be used in. For example, nickel is often used as a catalyst in reforming processes, while iron, copper and manganese is better suited for combustion processes [4].

$$CH_4 + MO => 2H_2 + CO + M \tag{1.4}$$

$$M + CO_2 => MO + CO \tag{1.5}$$

For CLT to become a viable alternative to the conventional alternatives, there is a need for OC material which is chemically favorable for the intended reactions, economically feasible, environmentally friendly and has good reactivity and stability [9]. A significant issue in CLR is the deactivation of the OC material leading to lower product yield. Deactivation of the OC can be caused by many processes and some are irreversible. Sintering of the OC particle is an irreversible process which leads to a decrease in surface area as particles are fused together [4]. Deposition of carbon onto the OC material also reduce activity as it blocks the reactive surface, and reactions with impurities can lead to agglomeration and changes in the chemical composition and reactivity of the OC[6][9]. Reactions with impurities can be difficult to reduce as they can be inherent to the OC if a natural ore is used, or a part of the fuel intake. Sintering may occur with most particles at the elevated temperatures used in CLT and can be reduced by using a thermally stable support material such as alumina, zirconia, etc [9]. Sintering can also be decreased by choosing a nanofibrous structure which has an inherent resistance to sintering [5]. The deposition of carbon can also be difficult to prevent but may be reduced by choosing suitable material composition and morphology[10]. Carbon depositions can also be oxidized into CO_2 in the air reactor which will regenerate the OC activity [6].

Nickel-based OC has been used successfully in CLR processes and is often considered the best metal to be used for this purpose [6]. While it is very suitable for the CLR process, it does face issues with carbon deposition, high costs and toxicity [4] [6]. Iron is a possible alternative to nickel and has been extensively studied as it is relatively inexpensive, abundant and environmentally safe [11]. Iron-based OC, are not without issues of their own. As iron oxides are reduced, Fe-ions tend to migrate towards the OC particle surface which can cause sintering [11]. Iron-based OC also have issues with carbon deposition and reactions with impurities much like their nickel-based counterparts, while also being less effective than nickel in methane reformation [4]. A possible way to improve the effectiveness of iron-based OC in CLR could be to dope the OC material with other metals and add a stable support material to reduce sintering. Several studies have been conducted to explore the effects of dopants and supports in OC material and this generally leads to an improvement in activity [4] [11] [12].

With the above mentioned research in regard, this thesis will attempt to synthesize a nanofibrous alumina-iron-based OC material doped with different metals to achieve a stable and effective OC. To evaluate the OC material, its morphology, stability and efficiency in dry methane reforming will be investigated.

1.2 Aim

The aim of this study is to synthesize and evaluate the stability and activity of Fe_2O_3/Al_2O_3-based nanofibrous OC in methane reforming and also study how some dopant metals affect the OC properties.

2
Theory

Iron is chosen as the main active element in the OC for this project. It exhibits suitable properties for CLR and is both inexpensive, non-toxic and abundant. The pure metal has two different oxidation states (Fe^{2+} and Fe^{3+}), can easily react with oxygen and can form several different oxides (FeO, Fe_2O_3 and Fe_3O_4) with varying concentrations of oxygen which can be important in partial oxidation processes like CLR [13].

Alumina is an aluminium oxide (Al_2O_3) that occurs naturally in many minerals. It is chemically stable, has a high melting point ($\approx 2030°C$), and can be manufactured with different morphologies [14]. Alumina has previously been used as a support material for metal impregnation in the synthesis of OC material. A significant drawback of using alumina as a support is the reaction between the active elements and the alumina which form aluminates (In the case of iron, iron aluminate, $FeAl_2O_4$, is formed). This will generally decrease the OC activity as the aluminates have a lower oxygen storage capacity. This can be resolved by deliberately forming aluminates in the support material prior to impregnation, or by using an excessive amount of active material so that the loss from aluminate formation is negligible [4].

Cerium is a very reactive lanthanide metal and is the most abundant of the rare-earth metals. Cerium is currently used in catalytic applications [15] and has previously been tested as a dopant in OC material where it increases activity and [12] [11]. Studies of Cerium-doped iron-alumina OC showed promising results with increased resistance to the formation of carbon deposits [4].

Strontium is an alkaline earth metal that is relatively abundant and very reactive [16]. Doping of iron-based OC with strontium has previously been studied in CLC applications where it promoted reactivity and cyclic stability of the OC[11].

Manganese is a widely distributed metal that is commonly used in steel manufacturing [17]. Manganese has a low price, is environmentally friendly and has many oxidation states, similar to iron. Manganese OC have been used in CLC and CLR applications, but it often reacts with support materials, which reduces the reactivity of the OC. Studies have also been conducted where manganese was used together with other metals which gave promising results in terms of stability and oxygen transport [4].

Nickel is commonly used in metallurgy for corrosion-resistant alloys, battery manu-

facturing, as catalyst material and much more [18] [19]. Nickel-based OC is generally considered the best material used for CLR processes as it has excellent oxygen carrying capacity and reactivity. However, nickel OC face severe issues with sintering and surface carbon deposition. Aside from these issues, nickel is quite expensive and excessive exposure to nickel can cause allergic reactions, kidney and cardiovascular problems and cancer. Nickel has been extensively studied for chemical looping processes and has been previously tested with electrospun nanofibrous alumina as a support material with promising results [20]. Although alumina can serve as a good support material for nickel OC it is important to consider the formation of nickel aluminate, as this will decrease the oxygen capacity and reactivity of the material [4].

2.1 Stabilization

Stabilization of the fibres samples is done before impregnation to enable the wetting of the fibres in the metal precursor solution, enabling a thorough impregnation of the fibres. Stabilization increases the stability and mechanical strength of the fibres by forming stable bonds in the polymer chains. The formation of these bonds occur in the temperature range between 200-300°C and is an exothermic reaction, which can lead to burning or deterioration of the fibres if the reaction temperature is too high, or heating time is too long [21].

2.2 Impregnation metal concentration

Iron will be used for the bulk of the active material in the OC used in this project and will be attached to the alumina support fibres by wet impregnation followed by calcination. The amount of iron in the impregnation solution was decided by studying the morphology of four samples impregnated with solutions with different iron concentrations. The concentrations of these solutions were 3.45, 2.58, 1.72 and 0.86 mol per liter. After studying the samples in a SEM microscope, a concentration of 0.345 mol per liter was chosen for impregnation beacause of excessive iron deposition at higher concentrations. Some samples will be doped with other metals to improve the efficiency of the OC materials. Considering previous studies where dopants have been used in OC material, a range of 2-5% weight seems appropriate for testing the effects of the dopant material [22][11], as higher amounts seem to have diminishing returns on efficiency [23].

2.3 Reformation temperature effects

Dry reformation of methane is an endothermic reaction and needs high temperatures (>600°C)to be carried out. Previous studies on iron-based OC suggests that temperatures above 800°C can increase the performance of the OC. Therefore, higher temperatures will be tested in this study [24] [12].

3
Method

3.1 Material selection

The materials used in this work have been selected in regard to their availability, price, reactivity and toxicity. While there are studies in which other materials are used with good results in CLR processes, these may have been overlooked because of rare, toxic or expensive material being used, which are less likely to be useful in large-scale processes. Alumina was selected for the nanofibrous substrate of the OC, and Iron has been selected as the main oxygen carrying constituent. The dopant metals chosen in this study are cerium, strontium, manganese and nickel. The different samples will hereafter be abbreviated according to table 3.1.

Sample	Abbreviation
Undoped alumina fibres	Alumina
Alumina impregnated with only iron	Pure Fe
Alumina impregnated with iron and cerium	Fe-Ce
Alumina impregnated with iron and strontium	Fe-Sr
Alumina impregnated with iron and manganese	Fe-Mn
Alumina impregnated with iron and nickel	Fe-Ni

Table 3.1: Sample constituents and abbreviations

3.2 Sample preparation through electrospinning

The fiber preparation method is largely based on an earlier report on alumina nanofiber preparation [25]. The precursor solution used in electrospinning of alumina nanofibres was prepared in a vial by adding polyacrylonitrile (PAN) to dimethylformamide (DMF) in a weight ratio of 10%. The solution was stirred for 12 hours using a magnetic stirrer to homogenize the solution. Aluminium acetyl acetonate (Alac) was then added to the solution in a 1:1 ratio to PAN, and the solution was stirred until clear. Initial small-scale testing of this worked well, but when upscaled to larger volumes additional DMF needed to be added for complete Alac dissolution. The clear solution was then transferred to 20 ml syringes with 18 gauge needles which were mounted into the electrospinning instrument. To facilitate the collection of the fibres, a sheet of aluminium foil was wrapped around the collecting cylinder. The edges of the sheet were affixed with tape so that only foil was exposed outwards.

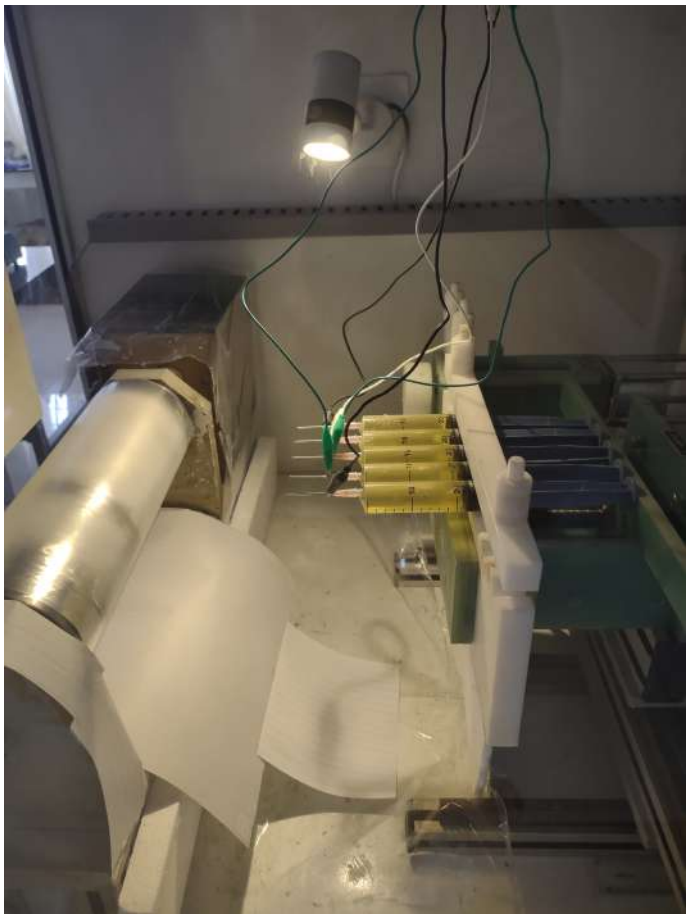

Figure 3.1: Inside setup of the electrospinning machine. Syringe pump with filled syringes can be seen on the right and the collector drum is seen to the left in the image.

The machine used for electrospinning was a PICO brand V2VH model, manufactured by Physics Instruments Co. Chennai, India. When spinning, the voltage was set to 18 Kv and was applied to the syringes by connecting the syringe tips to the power supply with cables. The collector rotation was set to ≈200 rpm and the extrusion to 1ml per hour. The distance between the collector and the syringes was 11 cm and the translation movement rate of the syringes was ≈ 0,16 meters per minute.
After the electrospinning was completed, the fibre sheet was removed from the collector by cutting the wrapping along the seam and unwrapping the cylinder. The collected fibres were removed from the foil and cut into pieces for easier loading into crucibles as seen in figure 3.2. The fibres were then stabilized by heating them in a tube furnace or muffle furnace at a temperature of 260°C for 2 hours with a heating rate of 5°C per minute. (These were the general settings. the stabilization of the fibres could become uneven, and the settings was sometimes changed depending on the oven used.) Correctly stabilized fibres would have a colour as shown in figure 3.3, but fibres of lighter colour would have to be heated again for reliable impregnation. Overheating could lead to carbonization of the material which is evident by the material becoming completely blackened. Carbonized material would not be

used for further sample preparation.

Figure 3.2: Unstabilized fibre sheet loaded into crucibles.

Figure 3.3: Stabilized fibres in crucible. While there is a clear colour gradient which indicates uneven stabilization, pieces within this colour span would reliably absorb the impregnation solution.

3.3 Wet impregnation

Impregnation solutions of metal precursors and water were prepared by mixing in a beaker. The stabilized alumina fibres were added to the solution until fully saturated and were then removed from the solution. It was important to use correctly stabilized fibres as incomplete stabilization would not allow the impregnation solution to wet the fibres as seen in figure 3.4

Figure 3.4: Poor wetting can be seen on fibres which have not been completely stabilized to the left. A piece of correctly stabilized fibres can be seen to the right in the dish which readily absorbs the solution.

Iron(III) nitrate nonahydrate was used to provide the iron in the impregnation solution, the target concentration of Fe^{3+} in the impregnation solution was 0,345 moles per litre. The target concentration of dopants was chosen as 0,069 mol/L, and the nitrate-hydrates of the various dopants was used in the solution preparation.

Table 3.2: Concentrations and masses of metals used in the impregnation solutions

Sample	**Fe^{3+} conc. (mol/L)**	**Dopant conc. (mol/L)**	**Metal loading (grams)**
Pure Fe	0.345	-	1.926 Fe
Fe-Ce	0.345	0.069	1.926 Fe, 0.96 Ce
Fe-Sr	0.3445	0.069	1.924 Fe, 0.6 Sr
Fe-Ni	0.345	0.0689	1.926 Fe, 0.4 Ni
Fe-Mn	0.3449	0.0691	1.926 Fe, 0.38 Mn

3.4 Calcination

The impregnated fibres were put into a crucible and heated in a furnace to 260°C with a rate of 5°C per minute to evaporate the water from the impregnation solution. After 1 hour dwelling time at 260°C, the temperature was increased to 950°C at a rate of 10°C per minute and held at 950°C for 2 hours to calcine the sample. The finished material were small delicate flakes with an orange colour, shown in figure 3.5. Some of the flakes could have a metallic surface, possibly due to excessive metal loading, as seen in figure 3.6.

Figure 3.5: Finished material, the sample shown is only impregnated with iron.

Figure 3.6: Finished material impregnated with iron and cerium. Note the metallic gray piece at the centre, possibly indicating excessive metal loading.

3.5 Reactivity testing

To test the reactivity of the samples, approximately 1,5 grams of calcined impregnated sample was loaded into a reactor tube made of quartz glass. The tube has a glass membrane to keep the OC bed in place in the middle of the tube. The ends of the tube are closed with two caps, in which there are glass sleeves for thermocouple insertion and inlet/outlet tubes to feed the reaction gas through. The connections between the main reactor tube and the caps was sealed with high vacuum grease to ensure a complete seal. A fixed bed setup was chosen for the reactivity testing. With this setup, the gas was fed from the top of the tube and out of the bottom, and the material remained in place on the glass membrane. This setup was chosen because the OC material had a very low density and was very likely to escape the reactor with the exhaust gas if the gas had been fed from the bottom of the reactor. The resulting exhaust gas was sent through a gas analyzer (Emerson NGA 2000) to determine the concentration of CO, CO_2, CH_4, O_2 and H_2. The data was then used to compare the reactivity and calculate the efficiency of the different materials. A gas flow of 0,7 L/min was chosen for the material testing experiments, the composition of the gas was regulated with mass flow controllers. To get some baseline values for later calculations, the gas output concentrations of a cold reactor was tested and shown to be $\approx$ 9.3% CO_2 in nitrogen during the oxidation, $\approx$5,2% CH_4 in nitrogen during reduction and pure nitrogen being used as a purge gas between the cycles. The duration of the oxidation step in the cycles was 400 seconds, the reduction was

300 seconds, and the nitrogen purge was 180 seconds. As fresh material often needed a few cycles to become activated, the initial cycles would be excluded from the data. Each type of material was tested in this way and the used samples was collected for further study. Further description of the system that was used can be found in [26]. After some initial experiments on the pure iron sample had been completed, the temperature span of 850-1000°C was deemed suitable for testing, as lower temperatures gave little to no reactivity. This temperature span was tested in 50°C increments and the material was put through at least three cycles at each temperature. In addition to these tests some further testing was performed on some fresh stontium and nickel samples. In these tests, the temperature was set to 950°C, oxidation and reduction phases were extended, and the concentration of methane was increased.

3.6 Scanning electron microscope analysis

To study the morphology and composition of the OC, a scanning electron microscope (Quanta 200 ESEM FEG) was used. SEM utilizes the small wavelength of electrons to get high resolution images of nanoscale materials. The SEM microscope used an electron emitter to focus an electron beam onto a sample, the electrons penetrate into the sample surface and interacts with the atoms present in the sample. The electron-sample interactions generate backscattered and secondary electrons together with characteristic X-rays. The resulting electrons are then detected and the information is used to generate an image of the sample, and the X-rays are used to analyse the sample composition [27]. The material that had previously been used in the reactor testing often had carbon depositions on the surface. To evaluate the effects of the reactor testing on the material, some of the used material was heated to 950°C in atmospheric conditions to remove these carbon deposits. This made it possible to compare the fresh material with the used samples, both with and without carbon deposits. To analyze the samples, a piece of double sided tape was attached to a specimen mount. A small amount of fibre sample was placed on the double sided tape and pressurized air was used to remove particles that had not adhered to the tape. The specimen mount was put into a sample holder which was inserted into the SEM instrument.

4

Results

The initial testing of the materials showed that all of the materials worked for DRM to some extent and using the SEM instrument, the successful synthesis of nanofibrous samples was confirmed. The nickel sample seems to be the most efficient, reaching the highest CO output in oxidation, and high H_2 output during reduction. The strontium doped sample performed second best of the doped samples, while the manganese doped sample was the least efficient, although it was better than the undoped sample in some regards. The undoped alumina sample performed surprisingly well in regards to the hydrogen production during reduction, which is most likely due to its ability to store carbon deposits on its surface, this was a property shared by all of the materials. The initial tests had a duration of ca. 22 oxidation-reduction cycles. Due to time constraints these were not extended any further.

4.1 Plots from initial testing

Plots of the outlet concentrations from the reactor are shown in the figures below. All of the samples had quite stable performance over the duration of the initial testing. The leftmost curve in each plot is the oxidation phase and the following curve is the reduction phase, separated by an inert phase. During the oxidation phase, CO_2 is being converted into CO as oxygen is being stored in the OC material. The CO_2 may also react with any carbon deposition on the OC surface to produce CO. In the reduction phase, CH_4 reacts with stored oxygen in the OC to produce H_2 and CO. The methane can also be converted into H_2 by deposition of carbon onto the OC material surface. This demonstrates the need for further testing of some materials. As the temperature was increased, the overall activity of the materials also increased. In figures 4.5 and 4.6, it can be seen that the baseline input of 9.3% CO_2 was not reached in the oxidation phases at higher temperatures, which affected the reactivity of these samples. Another noteworthy result from these tests was the gradual increase in hydrogen output for the duration of reduction phases, this was most evident in the high temperature cycles of the metal impregnated samples, shown in figures 4.2 to 4.6.

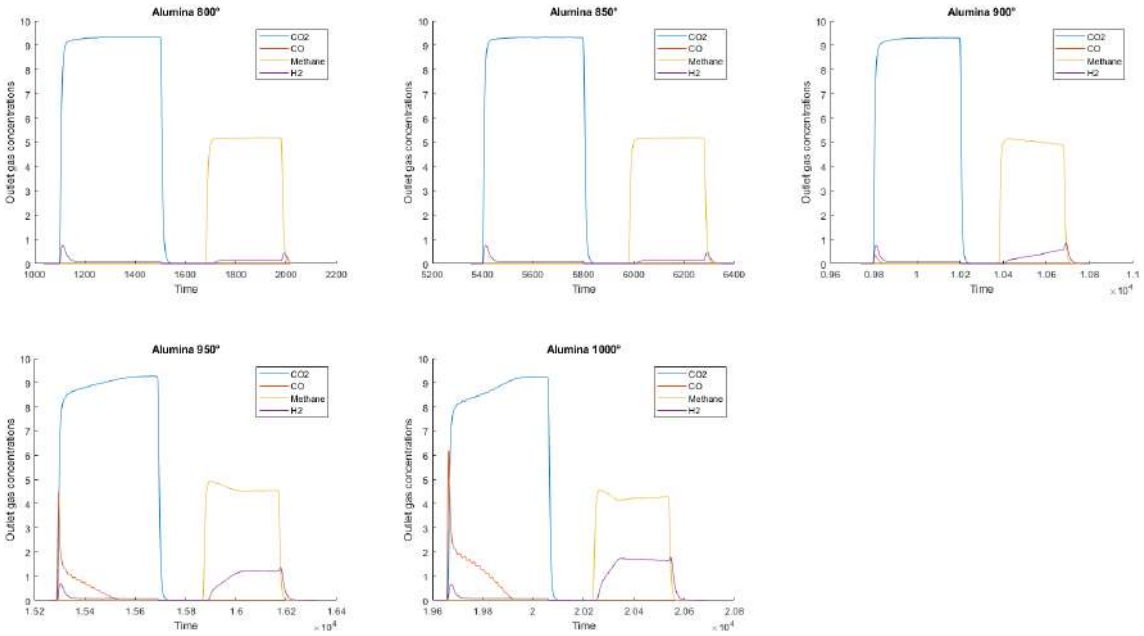

Figure 4.1: These plots correspond to the alumina fibre sample. N.B.: the lack of CO output during the reduction phase.

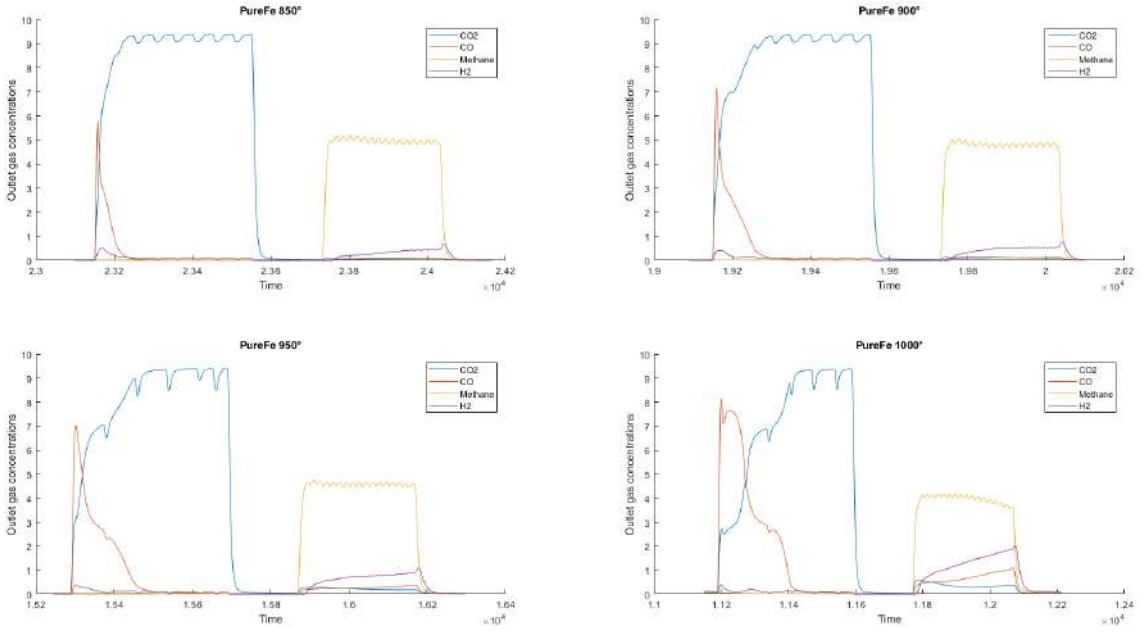

Figure 4.2: These plots correspond to the undoped sample using only iron and alumina, here denoted as then "PureFe" sample. The "waves" seen in the plots are a result of some initial issues with the system, which was resolved before the testing of the other samples. This issue did not affect the results of the experiment.

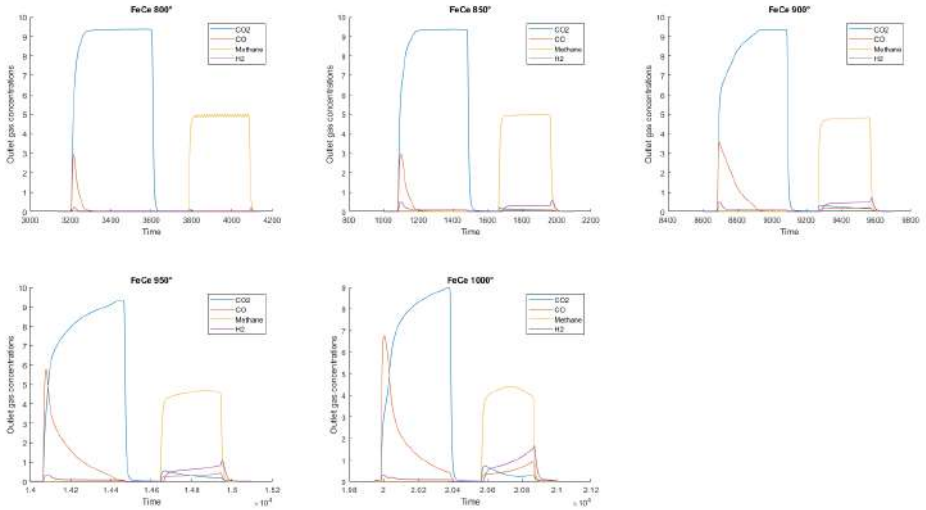

Figure 4.3: These plots correspond to the Cerium doped sample

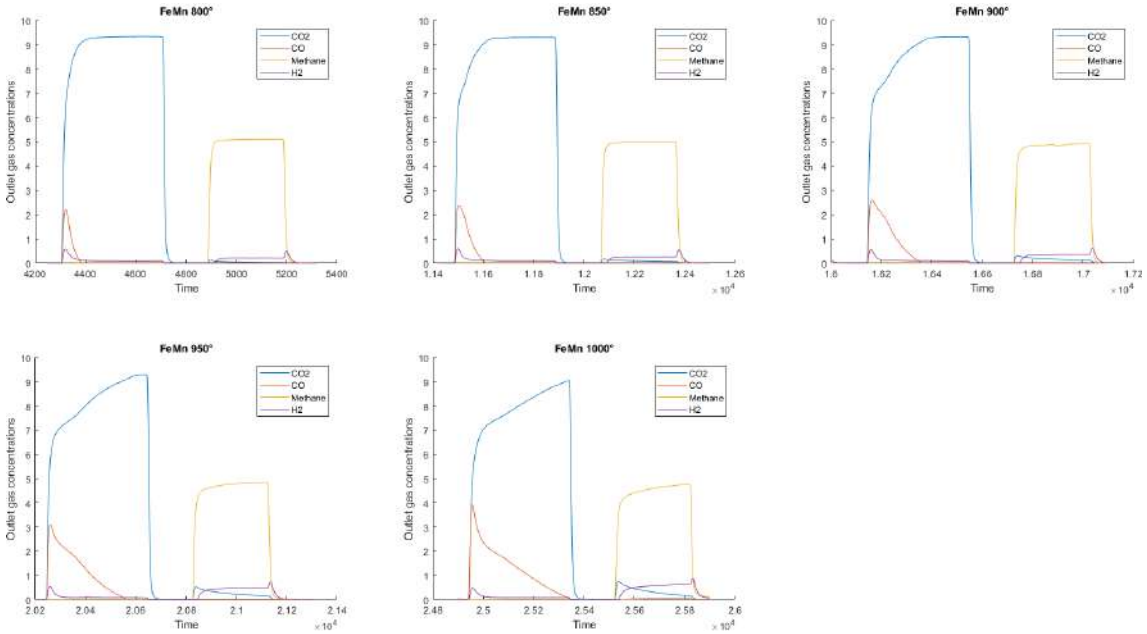

Figure 4.4: These plots correspond to the Manganese doped sample

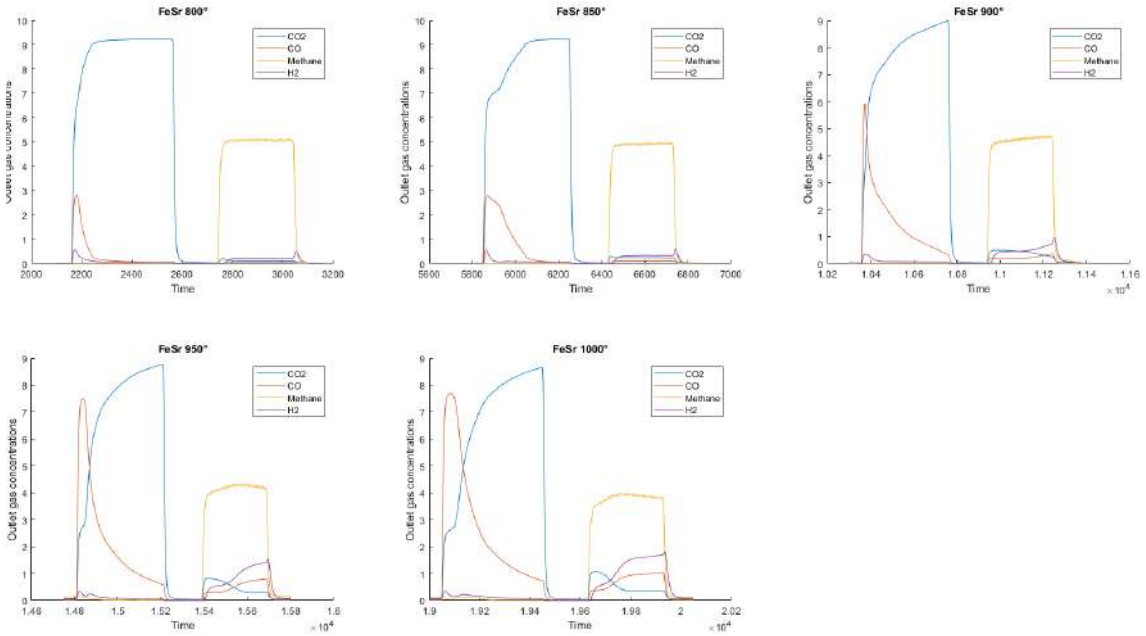

Figure 4.5: These plots correspond to the Strontium doped sample. N.B.: At 950 and 1000°C the concentration of CO_2 did not reach the baseline level of $\approx 9.3\%$, meaning the sample was not fully oxidized.

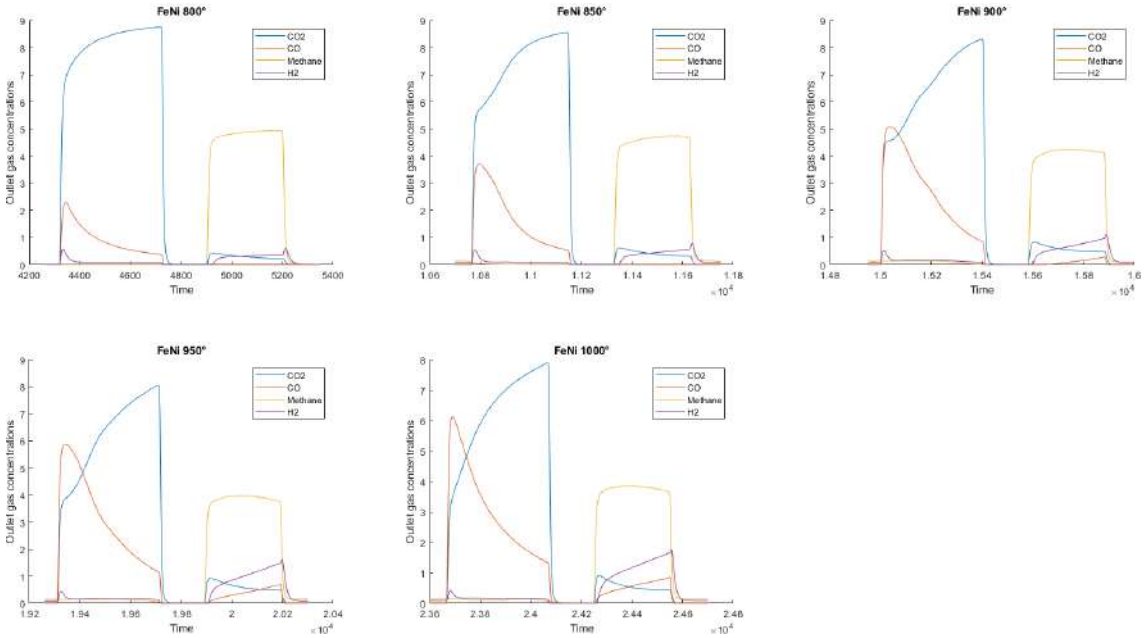

Figure 4.6: These plots correspond to the Nickel doped sample. N.B.: Much like in the Strontium doped sample, the CO_2 concentrations did not reach the baseline level, meaning the sample was not fully oxidized.

4.2 Molar exchanges and outputs of reactants and products

To get a rough estimate of how much gas is being converted in the cycles, the gas concentration measurements from a cold reactor was used as a baseline value of how much reactant was being put into the reactor at each cycle (shown in figure 4.7). The amount of converted reactants is then calculated .

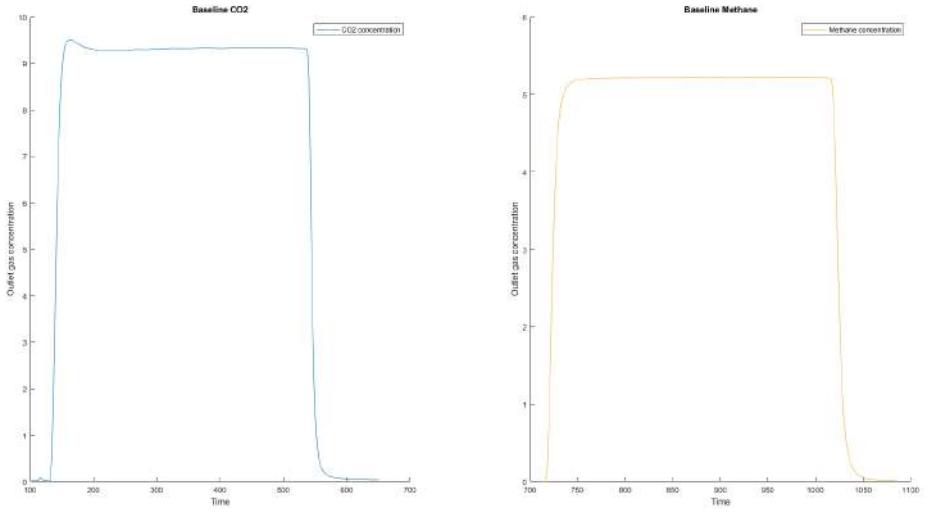

Figure 4.7: Diagram of the baseline gas concentrations

Table 4.1: This table contains some of the variables used in the gas exchange calculations

Variable	Value
Gas flow	0.0007 m^3/min
Pressure (p)	101325 pascal
Temperature (T)	298.15 Kelvin
Oxidation phase time	6.67 min
Reduction phase time	5 min
Oxidation phase CO_2 concentration	9.3%
Reduction phase CH_4 concentration	5.2%
Ideal gas constant (R)	8.3145 J/mol*K

The volume of gas input for both phases

$$0.0007 \cdot 5 = 0.0035m^3 \quad (reduction) \tag{4.1}$$

$$0.0007 \cdot 6.67 \approx 0.00467m^3 \quad (oxidation) \tag{4.2}$$

To caclulate the volume of reactants, the gas volumes are multiplied by the reactant fractions.

$$0.0035m^3 \cdot 0.052 = 0.000182m^3 = V_{CH_4} \tag{4.3}$$

$$0.00467m^3 \cdot 0.093 = 0,00043431m^3 = V_{CO_2} \tag{4.4}$$

Using the ideal gas law, the molar amounts of gas in each phase is calculated.

$$n = \frac{p \cdot V}{R \cdot T} \tag{4.5}$$

Table 4.2: Moles of gas fed into reactor in each cycle

Oxidation	0.0178 mol CO_2
Reduction	0.00744 mol CH_4

The molar amounts of gas in each phase are divided with the value of the integral of the corresponding phase graph in figure 4.7. The quotient from these equations acts as a conversion factor between the integral units and moles of gas. These conversion factors were used for their respective gases, and an average of the two factors were used in H_2 and CO molar calculations.

$$\frac{0.0178mol}{3780,26} = 4.7 \cdot 10^{-6} \quad (CO_2\ Conversion\ factor) \tag{4.6}$$

$$\frac{0.00744mol}{1570} = 4.74 \cdot 10^{-6} \quad (CH_4\ Conversion\ factor) \tag{4.7}$$

Integrating the CO, CO_2, H_2 and CH_4 plots from the initial sample tests and multiplying with the integral values with the corresponding conversion factor yields a product that represents the gas output of the cycles in moles. By using the conversion factors shown in equations 4.6 and 4.7 (and an average of the two for H_2 and CO calculations), the approximate output of the different gases is calculated according to equation 4.8. The molar outputs from the reactor during the different cycles in the initial tests are shown in figures 4.8 to 4.13.

$$Test\ integral \cdot Conversion\ factor = Gas\ output(mol) \tag{4.8}$$

When integrating the CO_2 and CH_4 plots from the initial sample tests and subtracting each phase with its corresponding baseline, the difference will represent the converted CO_2 and CH_4 in each test. By using the conversion factors shown in equations 4.6 and 4.7, this value is used to calculate the amount of converted reactants according to equation 4.9. The results of these equations are shown in figures 4.14a and b.

$$(Baseline\ integral - test\ integral) \cdot Conversion\ factor = converted\ reactants(mol) \tag{4.9}$$

The following diagrams show the output of CO, CO_2, CH_4 and H_2 depending on sample composition,oxidation/reduction phase, and the reactor temperature. The y-axis unit is mol, and represents the amount of gas in the output from the reactor. The samples preformed best at the higher testing temperatures, which was expected, as the DRM reactions are endothermic, and previous studies of iron based OC have shown better performance at high temperatures [24]. While all samples follow a similar trend of increasing reactivity as temperature increases, there was a notable decline in reactivity for the nickel doped sample at the higher temperature tests, and the strontium had a diminished increase of reactivity, as seen in figures 4.8, 4.9, 4.10 and 4.12. While the nickel and strontium samples were the most efficient in most regards, they also produced the most CO_2 by-product out of all of the samples in the reduction phase, as shown in figure 4.12. The strontium and cerium doped samples had the highest CO outputs during reduction phases at lower temperatures shown in figure 4.9, and strontium had the highest overall value, while cerium was surpassed at higher temperatures. This indicates a higher oxygen exchange between the OC and CH_4 for these materials. The pure Fe sample would sometimes have a higher efficiency than the doped samples, most evident in figures 4.8 and 4.12. This is surprising, as dopants usually will improve material efficiency [11]. At higher temperatures, the alumina sample had a high hydrogen output compared to the other samples, but it had very low CO output in both oxidation and reduction phases as seen in figures 4.8 and 4.12. This indicates that the reactions taking place are carbon deposition, and not the reforming reactions shown in equations 1.4 and 1.5.

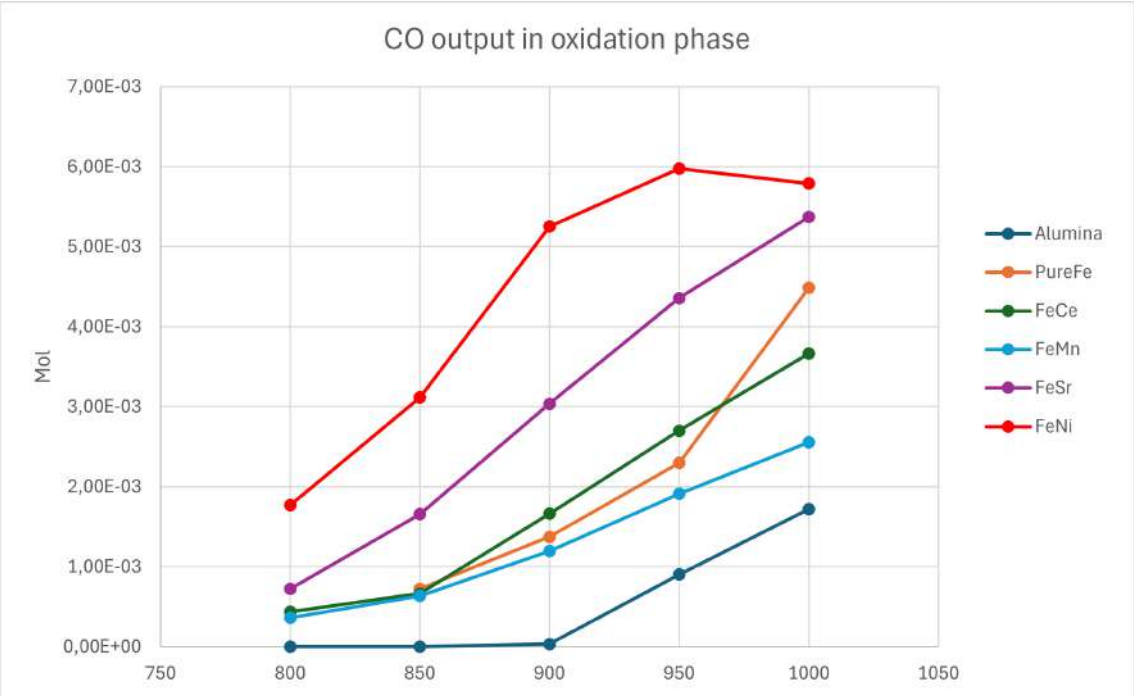

Figure 4.8: This diagram compares the CO output during the oxidation cycles. N.B.: the Nickel doped sample decreases in CO output.

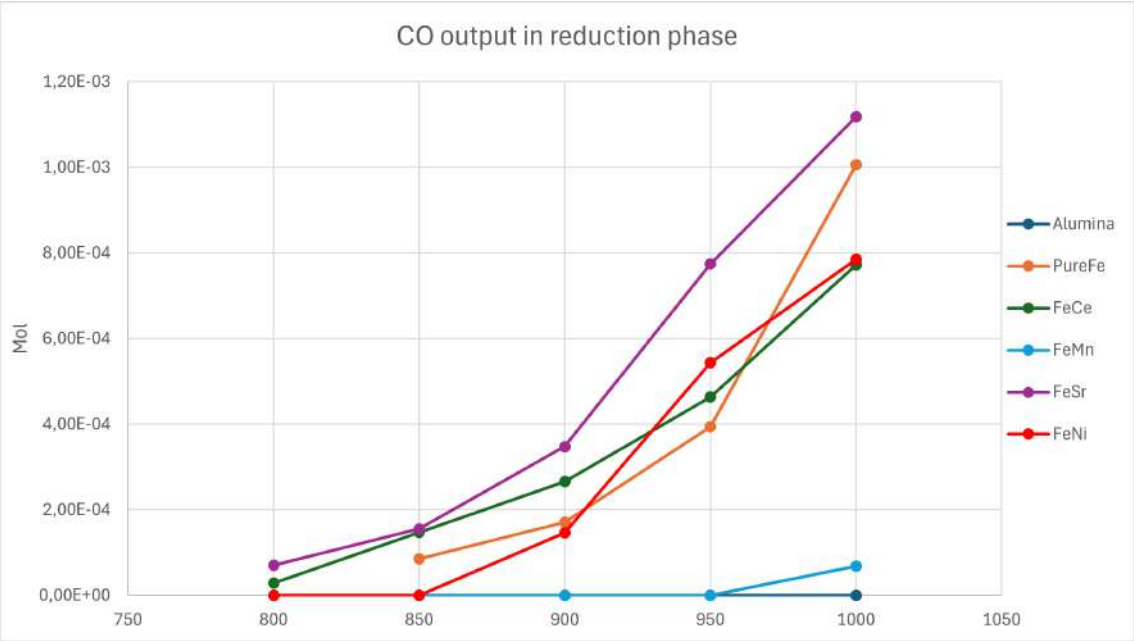

Figure 4.9: This diagram compares the CO output during the reduction cycles. N.B.:Alumina does not have any CO output in the reduction phase, and the Nickel doped sample does not follow the trend in increasing CO output as temperature increases.

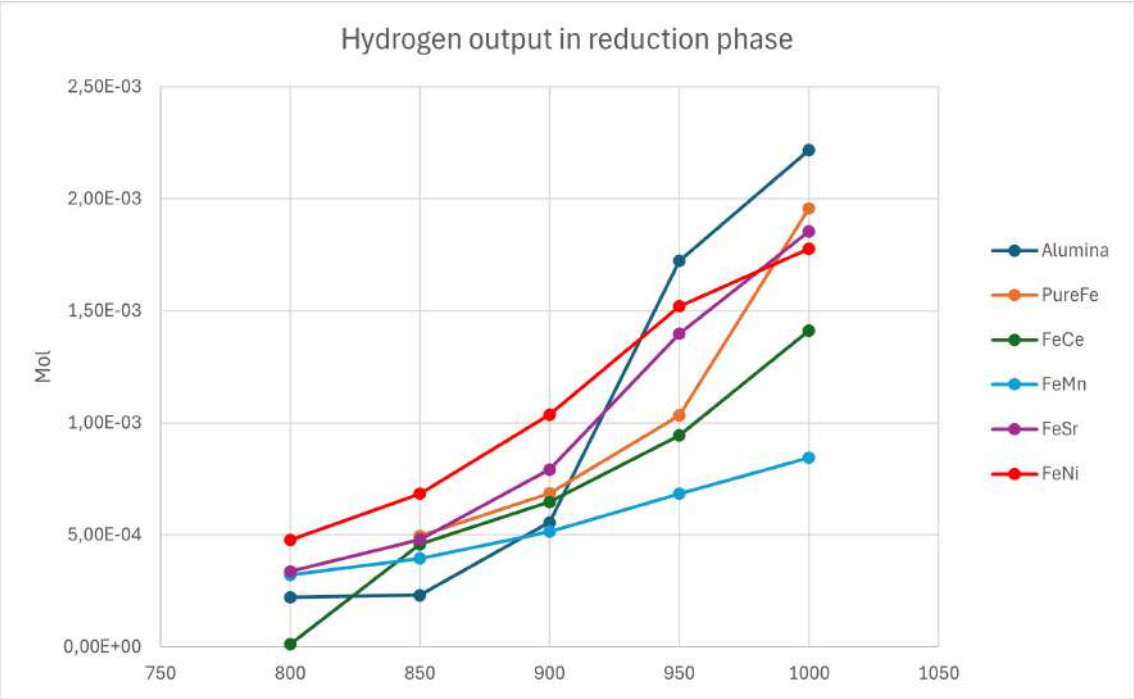

Figure 4.10: This diagram compares the H_2 output during the reduction cycles of the material.

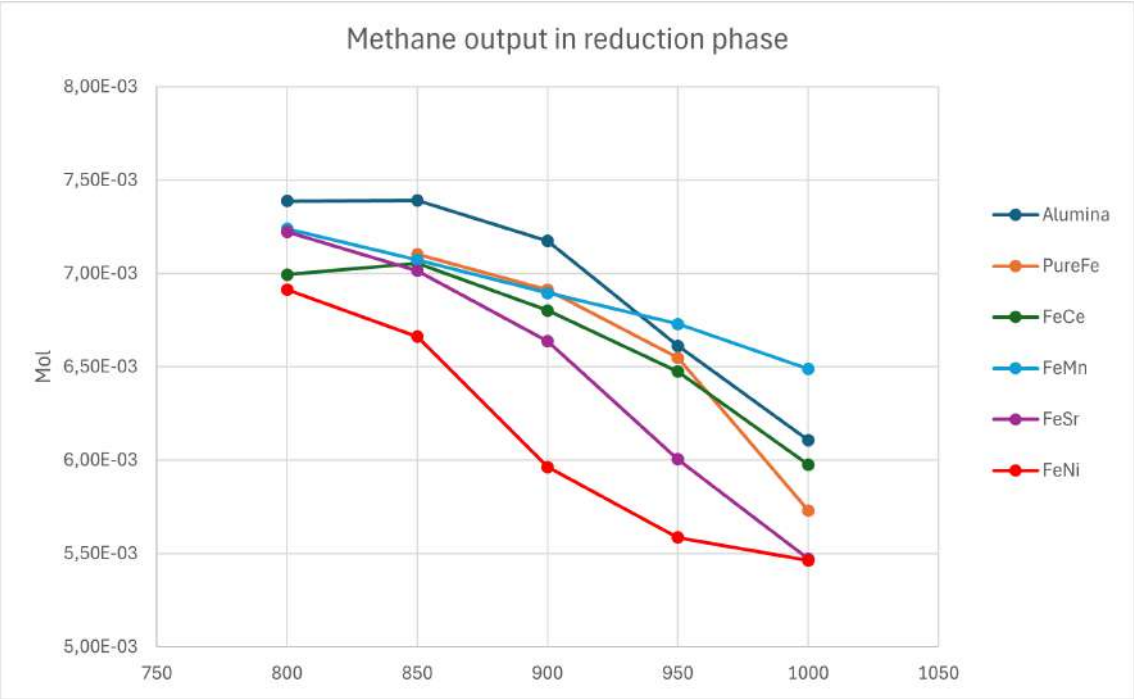

Figure 4.11: This diagram compares the CH_4 output during the reduction cycles of the material. As CH_4 is the reactant in the reduction phase, this value should ideally be as low as possible.

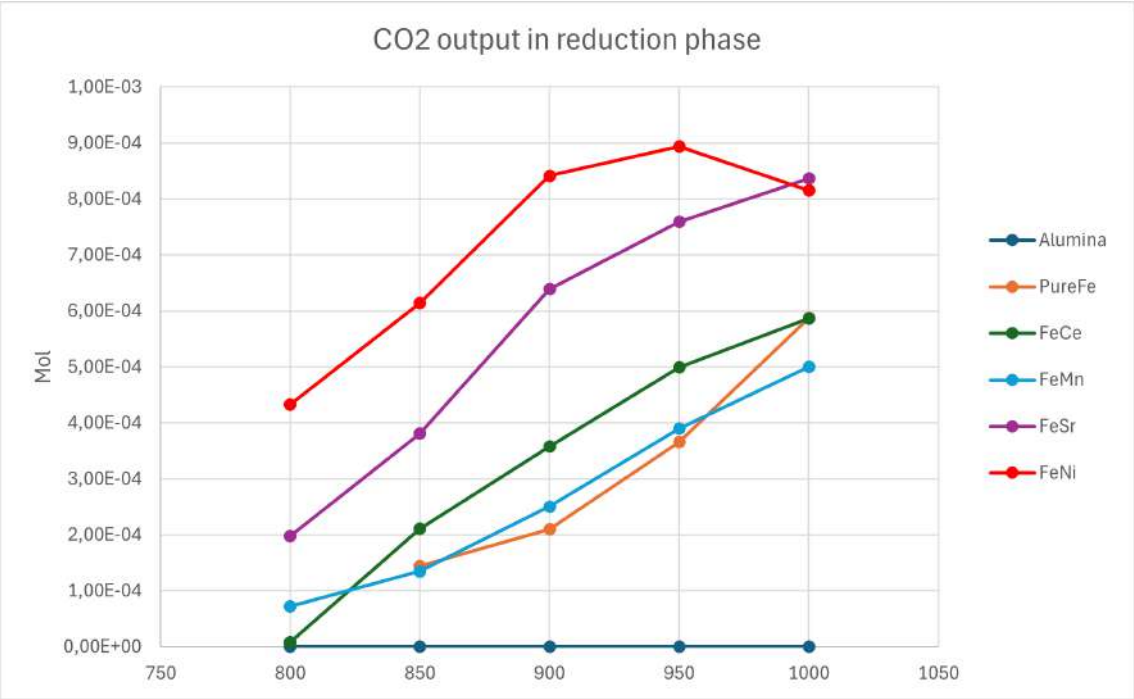

Figure 4.12: This diagram compares the CO_2 output during the reduction cycles of the material. As CO_2 is an undesirable by-product in the reduction phase, this value should ideally be as low as possible.

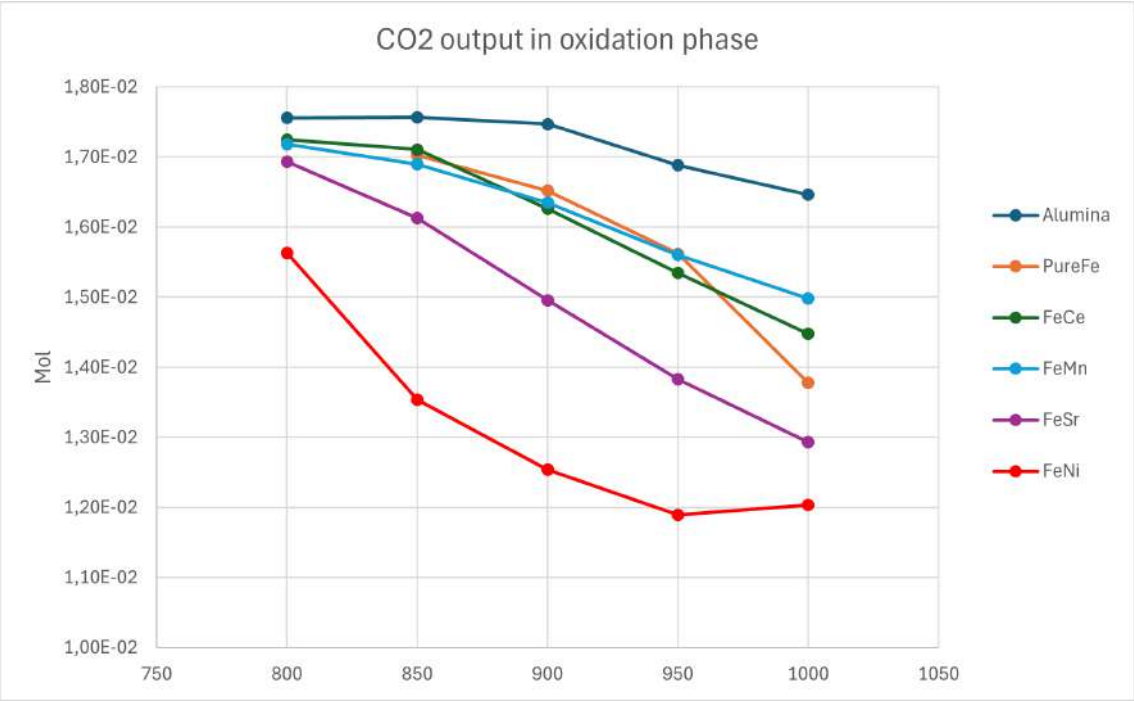

Figure 4.13: This diagram compares the CO_2 output during the oxidation cycles of the material. As CO_2 is the reactant in the oxidation phase, this value should ideally be as low as possible.

The amounts of converted reactants in each sample test is compiled in figure 4.14 a and b, with the corresponding data being available in figure A.1

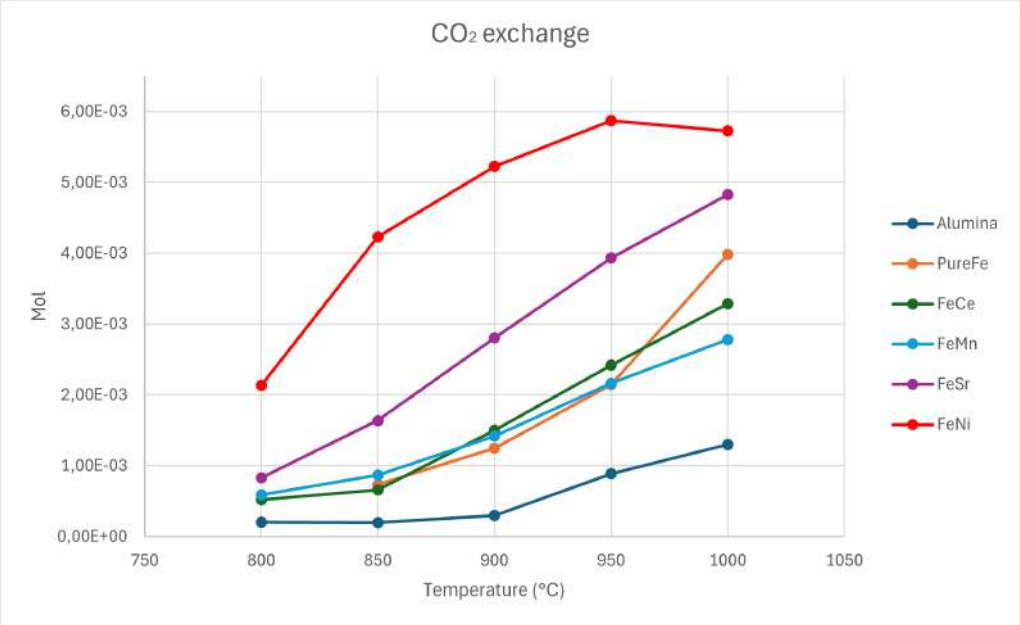

(a) CO_2 exchange in initial sample tests

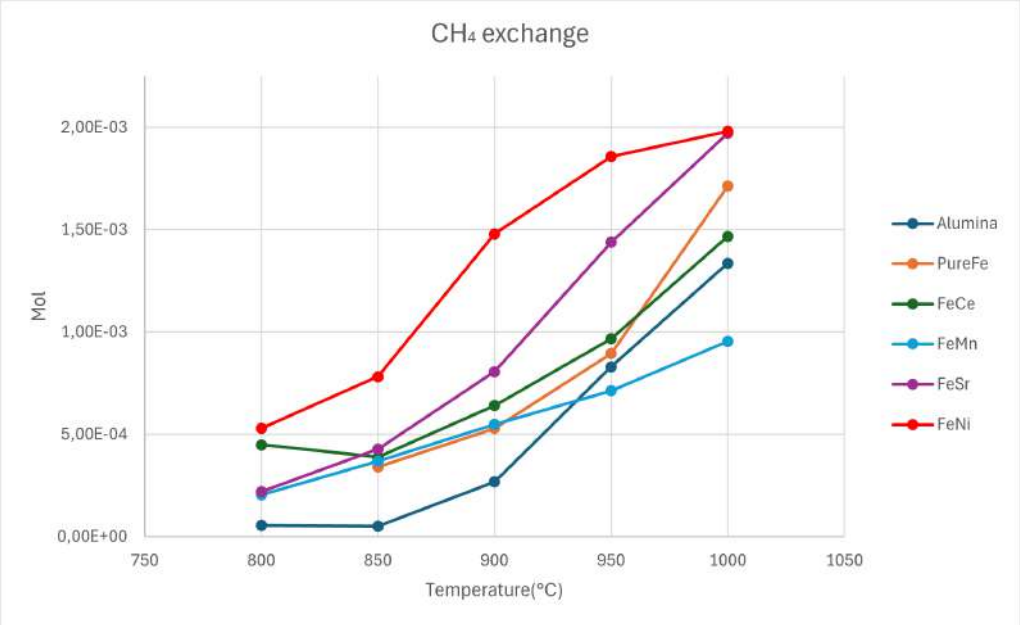

(b) CH_4 exchange in initial sample tests

Figure 4.14: Graphs of the reactant exchange in the initial tests

4.3 Further testing

The plots of the further testing experiments are shown below. In these plots, orange colour denotes CO_2, green CH_4, dark blue CO and light blue H_2 concentrations in the output gasflow from the reactor. These tests were made to evaluate how the samples performed during longer cycles than what was done in the initial tests. This was focused on the nickel and strontium doped samples as these seemed most promising based on the initial testing. The strontium doped sample showed stability even in the extended cycles and with increased concentrations, and the previously mentioned H_2 production during the reduction phase reached an eventual peak, and then slowly decreased as the reduction phase continued as shown in figures 4.15 and 4.16. There was a short CO output in the beginning of the reduction phases which would quickly reach low levels after the H_2 peak was passed. This indicates that the following H_2 production is an effect of carbon deposition, and not DRM reactions. This H_2 output would stabilize and slowly decrease over time after the peak had been passed, as shown in figure 4.16. Extended reduction phases also led to an increased output of CO in the oxidation phases. The nickel doped sample showed remarkable hydrogen production during the extended reduction phases shown in figure 4.17. Much like the strontium doped sample, it showed very low CO/CO_2 output during these phases, indicating that carbon deposition was taking place. The nickel doped sample also had a high CO output during the oxidation phases. During long cycle testing of a nickel doped sample, there was a sudden drop of gas flow through the reactor during the reduction cycle. This moment is shown in figure 4.19 and is indicated by a red arrow. This drop in gas flow could be an effect of excessive carbon deposition, blocking the gas flow through the material. The following sudden drop in hydrogen output and increase in CH_4 output was caused by diverting the gas flow directly to the analyzer, circumventing the reactor. This was done for a few seconds before redirecting the flow through the reactor again. This confirmed that the issue with the gas flow was caused by something in the reactor. Although the gas flow was lowered to below detectable levels in the analyzer, this bypass of the reactor showed that there was still some flow going through the reactor, which could be analyzed. While the data from the long reduction phase may be affected by this. The data before the decreased gas flow showed a similarly high H_2 output, indicating a high H_2 production up until this point, and possibly further.

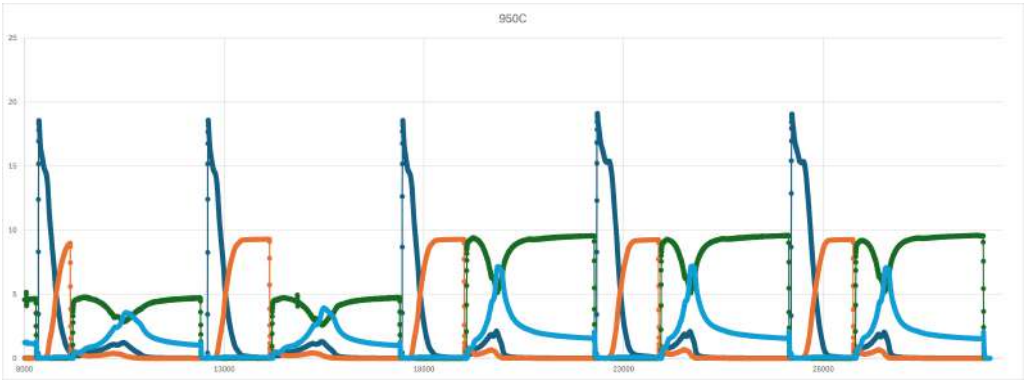

Figure 4.15: This graph shows some cycles from the cyclic stability testing of a strontium doped sample (activation cycles was excluded). The concentration of CH_4 was increased to 10% for the last cycles.

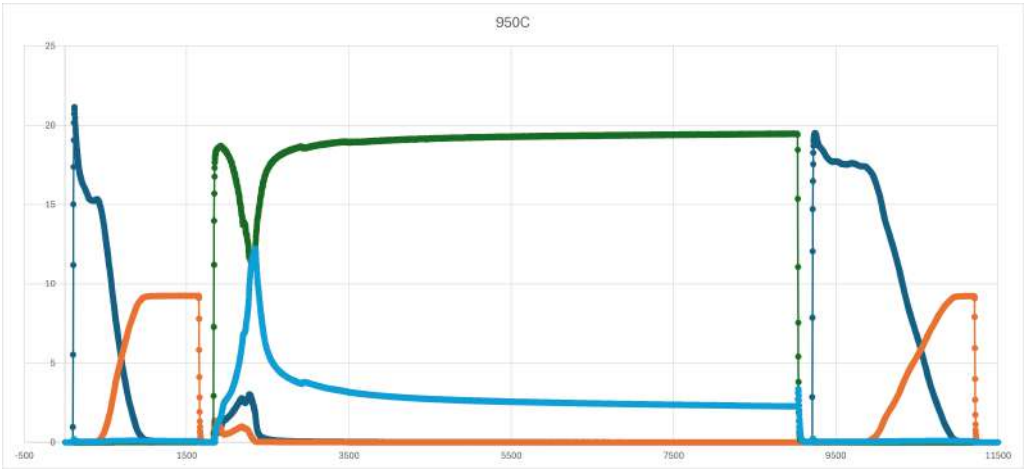

Figure 4.16: This graph shows the gas concentrations of the long cycle testing of a strontium doped sample.

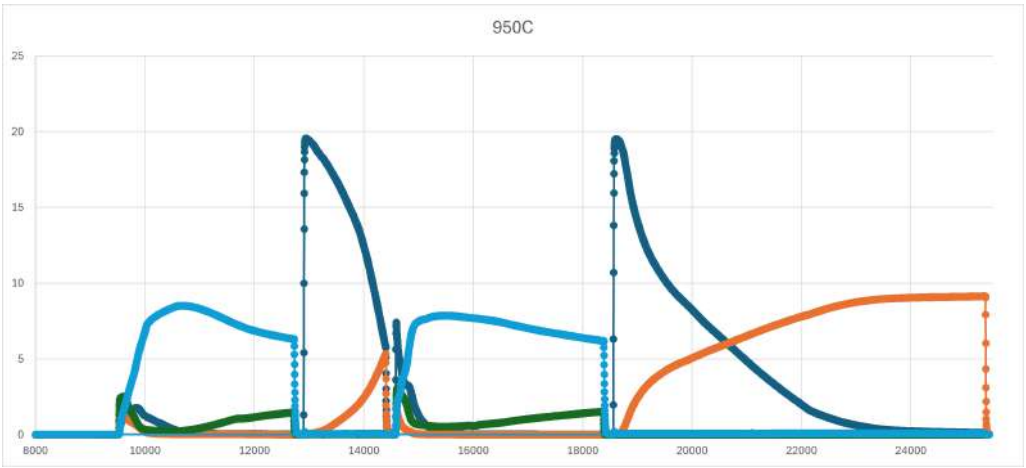

Figure 4.17: This graph shows the final cycles of the cyclic stability testing on the nickel doped sample.

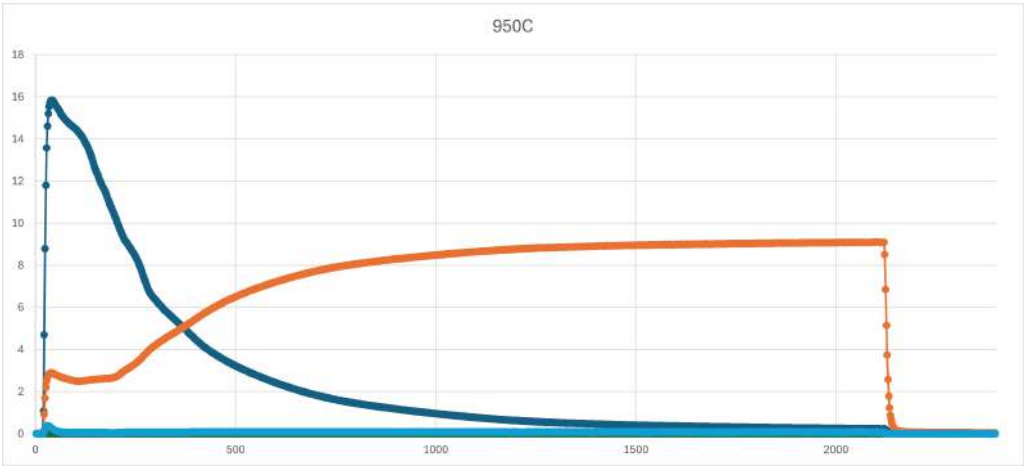

Figure 4.18: This graph shows the oxidation phase of a long cycle test on the nickel doped sample.

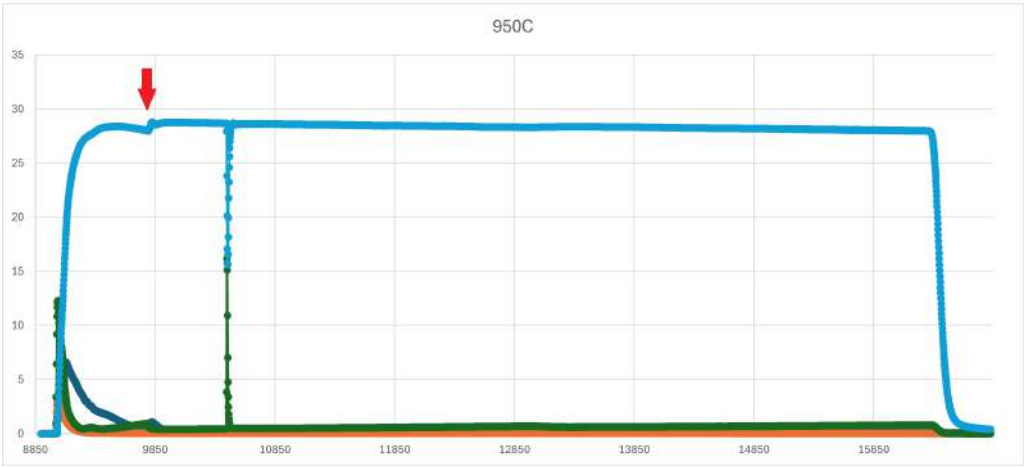

Figure 4.19: This graph shows the reduction phase of a long cycle test on the nickel doped sample. After some time, the gas analyzer showed a decrease of gas flow through the reactor. At the point marked with a red arrow, the flow dropped below detection limits, and the concentration values shown after this may be dubious.

4.4 SEM images

Below are some notable images captured by SEM analysis. More are listed in appendix figures A.2 to A.11. The images shown here are taken of fresh and used samples to evaluate the effects of using the materials in the reactor by comparing the images. There are also some images of used samples before decarbonization. The fresh metal impregnated samples that were analyzed with SEM had similar morphologies. The metal impregnated samples seemed to be similarly affected by the experiments, and although sintering had occurred on the samples, the fibrous structure would generally persist. The alumina fibre sample showed little to no change in material morphology as seen in figure 4.20, while the impregnated samples fibrous structure became less fine after use, as seen in figures 4.21, 4.22 and 4.23, with the nickel sample being the most affected as shown in figures 4.23a and b. The SEM analysis also showed that some parts of the samples had excessive metal loading on the surface, and therefore had no fibrous structure. An example of this can be seen in the left side of figure 4.24a (or in figure A.3 for a larger version of the image).

Notable effects of the more extensive long cycle testing was the fragmentation of material, sintering and the formation of very fine structures which is most clear in figure 4.23 c or A.11.. Due to time constraints, it was not possible to analyze all of the samples in SEM, it is possible that there are some notable morphology differences in the samples that have not been analyzed.

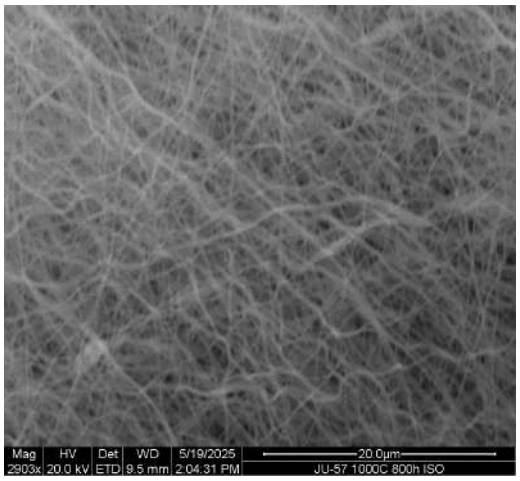

(a) This is a close-up image of alumina fibres without metal impregnation. They have not been used in any experiments.

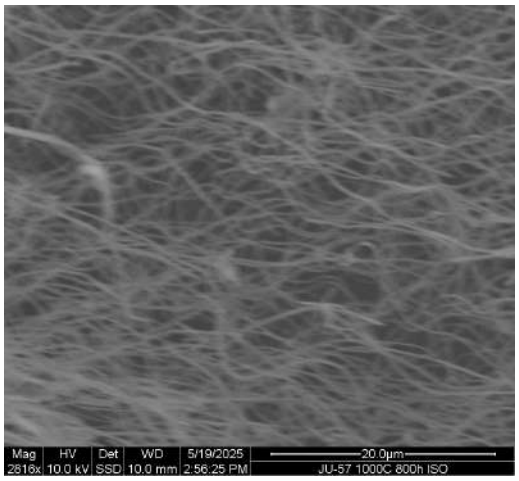

(b) This is a close-up image of alumina fibres without metal impregnation after they have been used in reactivity testing and decarbonized.

Figure 4.20: Alumina fibre samples before and after being used in the reactor

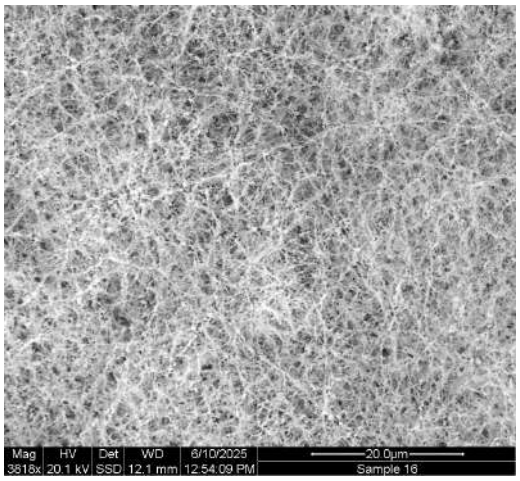

(a) Fresh pureFe sample

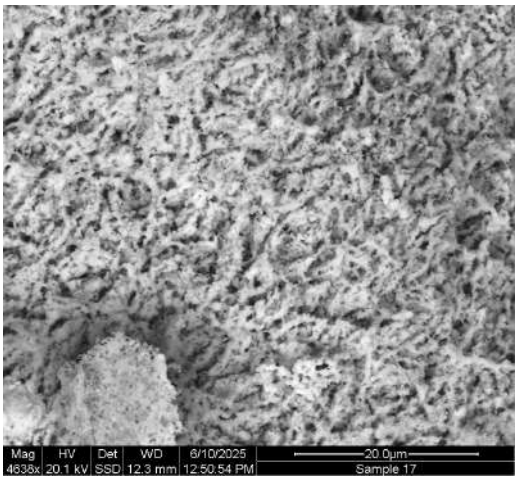

(b) Used pureFe sample with carbon deposition

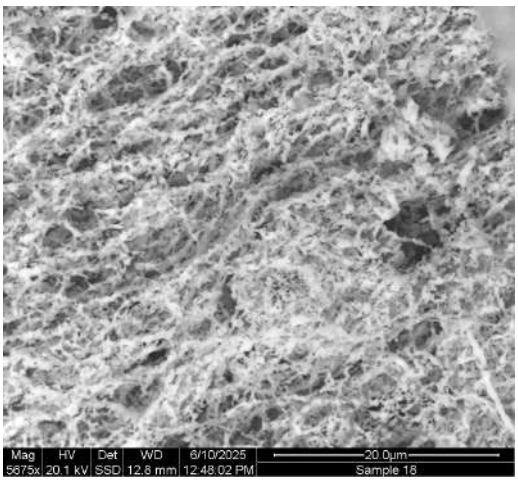

(c) This is a close-up image of alumina fibres impregnated with iron solution after being used in the reactor. The carbon deposition has been removed from this sample.

Figure 4.21: SEM images of PureFe samples

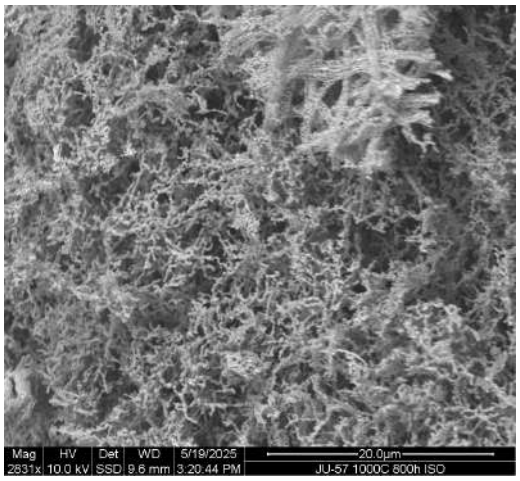

(a) This is a close-up image of a fresh cerium doped sample.

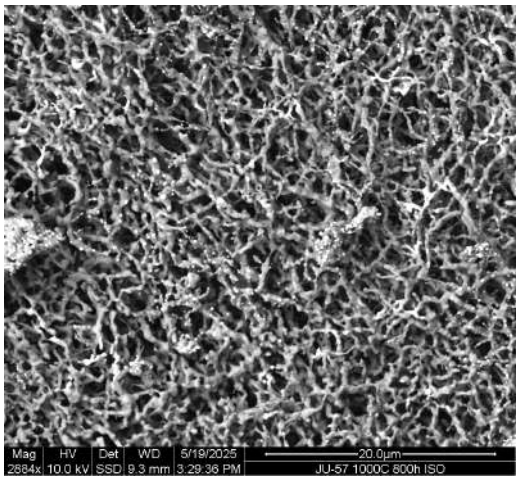

(b) This is a close-up image of cerium impregnated fibres after they have been used in reactivity testing but have not been decarbonized.

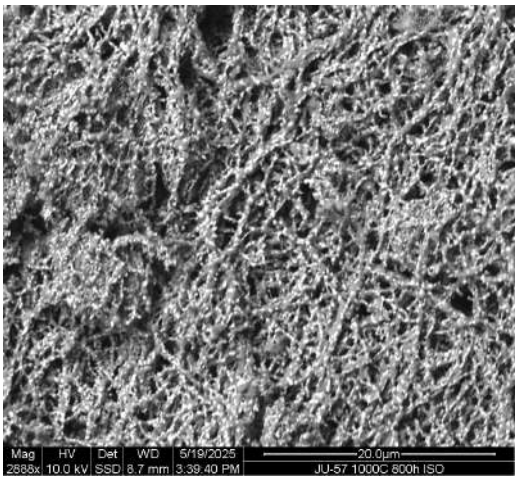

(c) This is a close-up image of cerium impregnated fibres after they have been used in reactivity testing and decarbonized.

Figure 4.22: FeCe samples before and after being used in the reactor

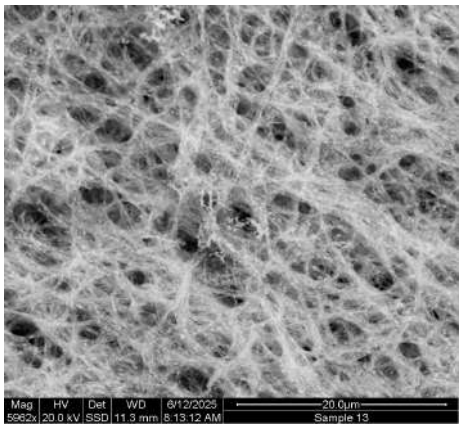

(a) Fresh FeNi sample

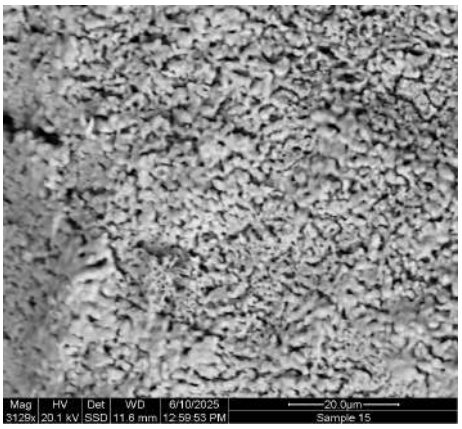

(b) Used decarbonized FeNi sample

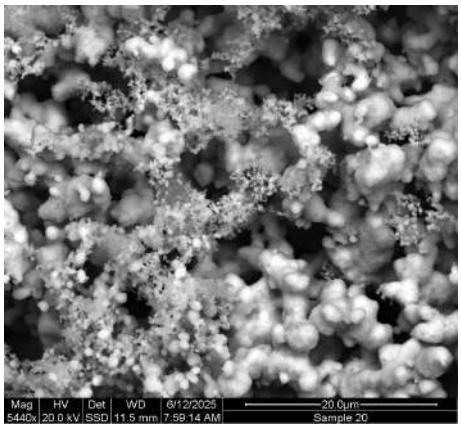

(c) Decarbonized FeNi sample from long cycle testing

Figure 4.23: SEM images of FeNi samples.

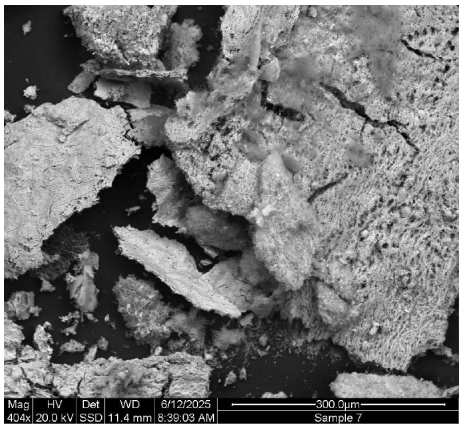

(a) Fresh FeSr sample. Some particles are more fibrous than others, this was common among all the impregnated samples.

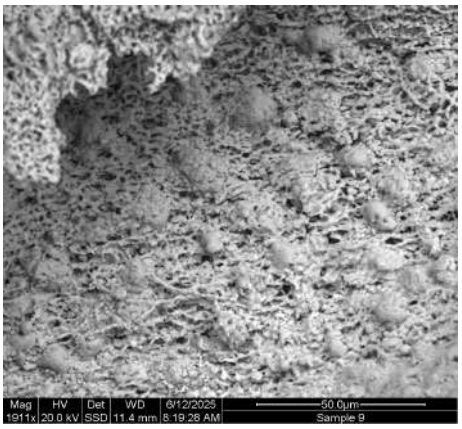

(b) Used, decarbonized FeSr sample.

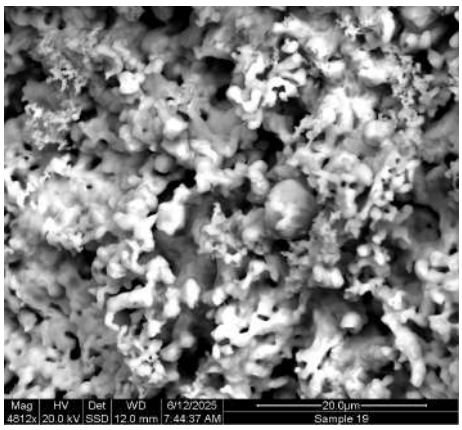

(c) Decarbonized FeSr sample used in the long cycle testing

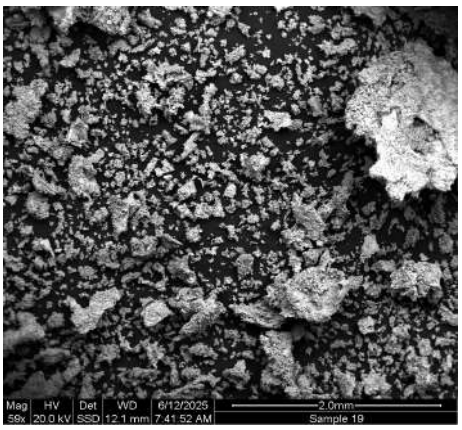

(d) Decarbonized FeSr sample used in the long cycle testing. After testing, many of the bigger particles had broken up into smaller pieces.

Figure 4.24: SEM images of FeSr samples

5
Discussion

The initial testing clearly showed that the nickel doped sample performed the best out of all the samples, followed by the strontium, and cerium doped samples. It is not surprising that the nickel doped sample performed the best, as nickel is already used in large scale methane reformation appliances. Nickel doped samples could be the best alternative when it comes to further implementation of this type of material. However, nickel is an expensive and somewhat toxic metal. The nickel doped sample used in the initial tests would also exhibit more extensive sintering than other samples. This may be due to the sample having less resistance to sintering, but more SEM analysis is necessary to confirm this hypothesis. The Fe-Ni sample used in the long cycle tests showed formation of some very fine fibres in the sample shown in figure A.11. This may be an effect of iron ion migration, which have been noted in previous studies [11].

Using strontium instead of nickel could be a better alternative, as the strontium doped sample had a high efficiency overall in the initial tests. Strontium is not as expensive as nickel and is also not toxic. It is still more expensive than the other dopants that were tested, and both the Fe-Ni and Fe-Sr samples would form CO_2 as a by-product to a higher degree than other samples. This CO_2 production took place in the beginning of the reduction phases and would decrease somewhat as time went on, but this process should be avoided or decreased if possible. Both the Fe-Ni and Fe-Sr samples needed longer oxidation cycles to be completely oxidized at the higher end of the temperature span of the initial tests, probably due to their higher reactivity. This likely affected the results of the initial testing. The decrease, and diminishing increase in efficiency for these samples shown in figures 4.8, 4.9, 4.10 and 4.14 is possibly caused by the sample not being completely oxidized, and it is very likely that they would otherwise have followed a trend similar to the other samples. In the further testing, the Fe-Ni and Fe-Sr was stable even in longer cycles, and extended reduction phases led to an increased output of CO in the oxidation phases. This is possibly a combination of more carbon deposition being converted into CO, and an increased oxygen exchange between the CO_2 and OC. This theory is supported by the characteristics of the Fe-Ni sample used in the further testing. The sudden drop in gas flow was probably due to extensive carbon deposition, and the used sample was difficult to remove from the reactor due to agglomeration, and blackened by carbon deposition.

Cerium worked quite well as a dopant and the resulting material was stable with a moderate efficiency overall. At 900°C the sample performed quite well compared to other samples, and SEM analysis showed that the cerium doped sample would retain most of its fibrous structure after the initial tests. However, more testing is

needed to study its longevity. Nevertheless, cerium is less expensive than strontium and is also non-toxic. More testing is needed to evaluate if it is better to use a less efficient but cheaper material rather than a more efficient and expensive one.
A surprising result from the initial testing is the high efficiency of the undoped alumina sample. This suggests that the nanofibrous structure of the samples plays a pivotal role in the efficiency of the samples. While the alumina sample did surpass the other samples in hydrogen production when used at high temperatures as seen in figure 4.10, it is important to note that this is only due to carbon deposition taking place, and not reformation. The molar exchange calculations makes this very clear, showing that the alumina sample was not as useful for CO_2 conversion reactions as the other samples. It is also not certain that the carbon deposition process is completely reversible, and may lead to permanent carbon deposits, which could inhibit this effect after some time (although this could be an issue with all of the samples). While the alumina sample was outperformed in most cases by the metal doped samples, it may still be useful for this application, as it would probably be cheaper to produce and handle, while showing a remarkable stability, with the fibres being seemingly unchanged by the initial testing, as seen in figure 4.20.
The manganese doped sample performed worst of the metal impregnated samples overall, but was still an improvement from the alumina sample when it comes to CO_2 and CH_4 exchange. This is not surprising as the addition of metals allows for the reformation reactions to take place, but it is interesting that its performance was worse or similar to the pure Fe sample. The addition of dopants usually improves the performance of an OC material, and there may be other reasons for its poor performance.
The pure Fe sample performance was about as what would be expected, but had a surprisingly high efficiency at the higher end of the temperature span, even surpassing that of the doped samples. However, as this was only the case at the higher testing temperatures, it may make it less efficient overall, as these temperatures could prove difficult to manage in large scale applications. But as iron is an inexpensive, abundant and non-toxic metal, it may prove viable for further applications, as this would reduce cost and make the handling of the material simpler.
As a side effect of the method used in these tests, the predominant output of CO and H_2 was separated between the cycles depending on if the cycle was in an oxidation or reduction phase. This may be of some use in larger scale productions, as it is not always desirable to get a mixture of these gases as a finished product.

5.1 Possible sources of error:

Due to time constraints, testing and analysis of all materials equally was not possible. The initial testing results are similar between the samples, with the exception of the pure Fe sample which was not tested at 800°C. However, the data from the pure Fe sample that was used should be as reliable as the data from the other samples. There was also some deposition of material on the reactor wall which was difficult to remove between tests. This deposition may have affected the results of some the experiments. Due to some samples not being analyzed with SEM, there is a possibility that the synthesis of some samples had failed, or at least been of lower quality than other samples. This may be the reason for the poor results of the manganese doped sample, but there was no indication of lesser quality from ocular inspection.
As the long reduction cycle of the nickel doped sample ran into some issues with the gas flow, the data from this experiment is dubious. However, the results from this experiments did show a high H_2 production before the decrease in gas flow, and this data can still be considered in the discussion.

6
Summary and conclusion

The materials synthesized in this thesis have shown to be a possible way to produce H_2 and CO. The materials seem to have benefitted from the addition of dopants, and the nanofibrous structure has played some part in the CO production due to its capacity to store carbon deposits for subsequent oxidation. SEM analysis showed that this method was a viable way to produce these kind of materials, however the metal loading could be adjusted to decrease excessive loading. The materials are listed in the table below in order of their efficiency.

Table 2 - From most effective resistant to least
1. Fe-Ni
2. Fe-Sr
3. Fe-Ce
4. Pure Fe
5. Fe-Mn
6. Alumina

The Fe-Ni and Fe-Sr samples generally had the highest output of the desired products, Fe-Ce was in the middle of the scale. PureFe performed well but was less effective at the lower temperatures, and the Fe-Mn sample was the least effective of the doped sample.
The undoped alumina sample could be utilized in this process, but it is not useful in a traditional DRM aspect. This material instead utilizes the material surface to bind and release carbon to produce the intended gases.

6.1 Further research

The excessive metal loading which was visible on some of the material makes further studies of material with decreased metal loading interesting. The effects of different dopant concentrations and different dopant combinations may also be interesting for further research. All of the samples used in this thesis could also be further investigated with more extensive reactivity testing and SEM analysis. If possible, the materials used in this thesis could also be tested in SMR reactions as iron has been extensively used SMR processes and these type of materials may be of use for that purpose [7].

Bibliography

[1] Anne Olhoff et al. *Emissions Gap Report 2024: No more hot air ... please! With a massive gap between rhetoric and reality, countries draft new climate commitments*. United Nations Environment Programme, Oct. 2024. ISBN: 9789280741858. DOI: 10.59117/20.500.11822/46404. URL: http://dx.doi.org/10.59117/20.500.11822/46404.

[2] Mikalai Filonchyk et al. "Greenhouse gases emissions and global climate change: Examining the influence of CO2, CH4, and N2O". In: *Science of The Total Environment* 935 (July 2024), p. 173359. ISSN: 0048-9697. DOI: 10.1016/j.scitotenv.2024.173359. URL: http://dx.doi.org/10.1016/j.scitotenv.2024.173359.

[3] O.A. Odunlami et al. "Advanced techniques for the capturing and separation of CO2 – A review". In: *Results in Engineering* 15 (Sept. 2022), p. 100512. ISSN: 2590-1230. DOI: 10.1016/j.rineng.2022.100512. URL: http://dx.doi.org/10.1016/j.rineng.2022.100512.

[4] Hao Zheng et al. "Chemical looping reforming: process fundamentals and oxygen carriers". In: *Discover Chemical Engineering* 2.1 (July 2022). ISSN: 2730-7700. DOI: 10.1007/s43938-022-00012-3. URL: http://dx.doi.org/10.1007/s43938-022-00012-3.

[5] Shailesh Singh Sikarwar et al. "A novel thermally stable Fe2O3/Al2O3 nanofiber-based oxygen carrier for chemical-looping combustion". In: *Chemical Papers* 76.6 (2022), 3987–3993. ISSN: 2585-7290. DOI: 10.1007/s11696-022-02129-9. URL: http://dx.doi.org/10.1007/s11696-022-02129-9.

[6] Rei-Yu Chein, Cheng-Yang Lu, and Wei-Hsin Chen. "Syngas production via chemical looping reforming using methane-based feed and NiO/Al2O3 oxygen carrier". In: *Energy* 250 (July 2022), p. 123815. ISSN: 0360-5442. DOI: 10.1016/j.energy.2022.123815. URL: http://dx.doi.org/10.1016/j.energy.2022.123815.

[7] Alberto Boretti and Bimal K. Banik. "Advances in Hydrogen Production from Natural Gas Reforming". In: *Advanced Energy and Sustainability Research* 2.11 (July 2021). ISSN: 2699-9412. DOI: 10.1002/aesr.202100097. URL: http://dx.doi.org/10.1002/aesr.202100097.

[8] Christopher Jensen and Melis S. Duyar. "Thermodynamic Analysis of Dry Reforming of Methane for Valorization of Landfill Gas and Natural Gas". In: *Energy Technology* 9.7 (May 2021). ISSN: 2194-4296. DOI: 10.1002/ente.202100106. URL: http://dx.doi.org/10.1002/ente.202100106.

[9] Shailesh Singh Sikarwar et al. "Performance assessment of novel nanofibrous Fe2O3/Al2O3 oxygen carriers for chemical looping combustion of gaseous

fuel". In: *Chemical Papers* 78.3 (2023), 1709–1717. ISSN: 2585-7290. DOI: 10.1007/s11696-023-03199-z. URL: http://dx.doi.org/10.1007/s11696-023-03199-z.

[10] Ashin A. Sunny et al. "Nanoscaled Oxygen Carrier-Driven Chemical Looping for Carbon Neutrality: Opportunities and Challenges". In: *Accounts of Chemical Research* 56.23 (Nov. 2023), 3404–3416. ISSN: 1520-4898. DOI: 10.1021/acs.accounts.3c00517. URL: http://dx.doi.org/10.1021/acs.accounts.3c00517.

[11] Zhong Ma et al. "Improved redox performance of Fe2O3/Al2O3 oxygen carrier via element doping in chemical looping combustion". In: *Fuel Processing Technology* 224 (Dec. 2021), p. 107030. ISSN: 0378-3820. DOI: 10.1016/j.fuproc.2021.107030. URL: http://dx.doi.org/10.1016/j.fuproc.2021.107030.

[12] Jinrui Zhang et al. "Enhancement of Fe/Ce oxygen carrier performance in chemical looping dry reforming of methane". In: *Fuel* 366 (June 2024), p. 131344. ISSN: 0016-2361. DOI: 10.1016/j.fuel.2024.131344. URL: http://dx.doi.org/10.1016/j.fuel.2024.131344.

[13] National Center for Biotechnology Information. *PubChem*. Accessed: 2025-02-13. URL: https://pubchem.ncbi.nlm.nih.gov/element/Iron.

[14] National Center for Biotechnology Information. *PubChem*. Accessed: 2025-02-13. URL: https://pubchem.ncbi.nlm.nih.gov/compound/Aluminum-Oxide.

[15] National Center for Biotechnology Information. *PubChem*. Accessed: 2025-02-13. URL: https://pubchem.ncbi.nlm.nih.gov/element/Cerium.

[16] Institute for rare earths and metals AG. *ISE*. Accessed: 2025-02-16. URL: https://en.institut-seltene-erden.de/seltene-erden-und-metalle/strategische-metalle-2/strontium/.

[17] National Center for Biotechnology Information. *PubChem*. Accessed: 2025-02-16. URL: https://pubchem.ncbi.nlm.nih.gov/element/manganese.

[18] National Center for Biotechnology Information. *PubChem*. Accessed: 2025-02-17. URL: https://pubchem.ncbi.nlm.nih.gov/element/nickel.

[19] Giuseppe Genchi et al. "Nickel: Human Health and Environmental Toxicology". In: *International Journal of Environmental Research and Public Health* 17.3 (Jan. 2020), p. 679. ISSN: 1660-4601. DOI: 10.3390/ijerph17030679. URL: http://dx.doi.org/10.3390/ijerph17030679.

[20] Li Liu et al. "Synthesis of a highly dispersed Ni/Al2O3 catalyst with enhanced catalytic performance for CO2 reforming of methane by an electrospinning method". In: *International Journal of Hydrogen Energy* 41.39 (Oct. 2016), 17361–17369. ISSN: 0360-3199. DOI: 10.1016/j.ijhydene.2016.07.151. URL: http://dx.doi.org/10.1016/j.ijhydene.2016.07.151.

[21] Ezgi Ismar and A. Sezai Sarac. "Oxidation of polyacrylonitrile nanofiber webs as a precursor for carbon nanofiber: aligned and non-aligned nanofibers". In: *Polymer Bulletin* 75.2 (May 2017), 485–499. ISSN: 1436-2449. DOI: 10.1007/s00289-017-2043-x. URL: http://dx.doi.org/10.1007/s00289-017-2043-x.

[22] Xinyi Chen et al. "Flame spray pyrolysis synthesized Ni-doped Fe/Ce oxygen carriers for chemical looping dry reforming of methane". In: *Fuel* 343 (July

2023), p. 127913. ISSN: 0016-2361. DOI: 10.1016/j.fuel.2023.127913. URL: http://dx.doi.org/10.1016/j.fuel.2023.127913.

[23] Bo Jin et al. "Low concentration Ni doping to intensify redox kinetics of iron-based oxygen carriers for efficient chemical looping reverse water gas shift". In: *Separation and Purification Technology* 360 (2025), p. 131237. ISSN: 1383-5866. DOI: 10.1016/j.seppur.2024.131237. URL: http://dx.doi.org/10.1016/j.seppur.2024.131237.

[24] Jesús Guerrero-Caballero et al. "Ni, Co, Fe supported on Ceria and Zr doped Ceria as oxygen carriers for chemical looping dry reforming of methane". In: *Catalysis Today* 333 (Aug. 2019), 251–258. ISSN: 0920-5861. DOI: 10.1016/j.cattod.2018.11.064. URL: http://dx.doi.org/10.1016/j.cattod.2018.11.064.

[25] Yu Ni et al. "Preparation of Electrospun Porous Alumina Nanofibers for Origami-Inspired Manufacturing". In: *Advanced Engineering Materials* 24.12 (Oct. 2022). ISSN: 1527-2648. DOI: 10.1002/adem.202201183. URL: http://dx.doi.org/10.1002/adem.202201183.

[26] Henrik Leion, Volkmar Frick, and Fredrik Hildor. "Experimental Method and Setup for Laboratory Fluidized Bed Reactor Testing". In: *Energies* 11.10 (Sept. 2018), p. 2505. ISSN: 1996-1073. DOI: 10.3390/en11102505. URL: http://dx.doi.org/10.3390/en11102505.

[27] Anwar Ul-Hamid. *A Beginners' Guide to Scanning Electron Microscopy*. Springer International Publishing, 2018. ISBN: 9783319984827. DOI: 10.1007/978-3-319-98482-7. URL: http://dx.doi.org/10.1007/978-3-319-98482-7.

A

Appendix

Converted CO2 in oxidation phases (mol)						
	Alumina	PureFe	FeCe	FeMn	FeSr	FeNi
800	2,05E-04		5,18E-04	5,87E-04	8,32E-04	2,13E-03
850	1,98E-04	7,38E-04	6,59E-04	8,70E-04	1,64E-03	4,23E-03
900	2,97E-04	1,25E-03	1,50E-03	1,42E-03	2,81E-03	5,22E-03
950	8,85E-04	2,15E-03	2,42E-03	2,16E-03	3,94E-03	5,87E-03
1000	1,30E-03	3,98E-03	3,29E-03	2,78E-03	4,83E-03	5,73E-03

(a) CO_2 exchange in initial sample tests

Converted CH4 in reduction phases (mol)							
	Alumina	PureFe	FeCe	FeMn	FeSr	FeNi	
800	5,51E-05		4,49E-04	2,04E-04	2,19E-04	5,28E-04	
850	5,09E-05	3,41E-04	3,88E-04	3,69E-04	4,28E-04	7,82E-04	
900	2,68E-04	5,29E-04	6,41E-04	5,48E-04	8,06E-04	1,48E-03	
950	8,30E-04	8,94E-04	9,67E-04	7,13E-04	1,44E-03	1,86E-03	
1000	1,33E-03	1,71E-03	1,47E-03	9,54E-04	1,97E-03	1,98E-03	

(b) CH_4 exchange in initial sample tests

Figure A.1: Tables of the converted amounts of reactants in the initial testing cycles

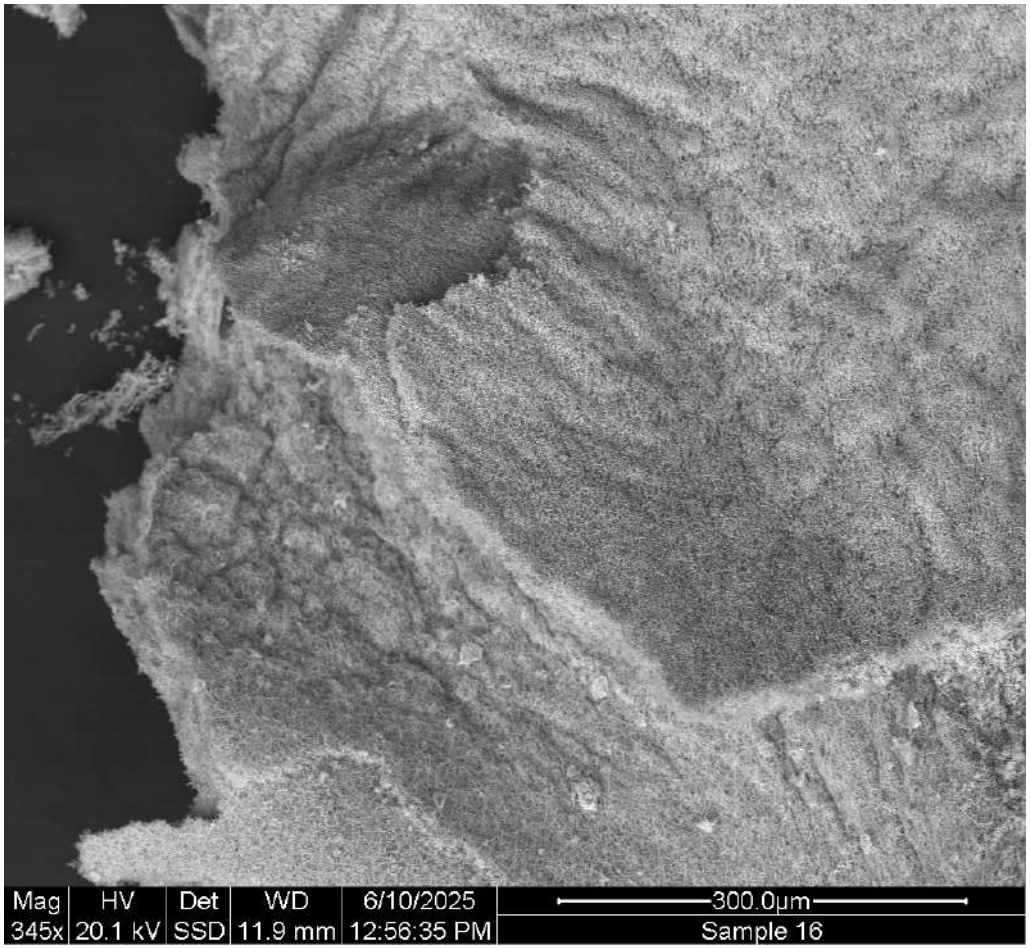

Figure A.2: SEM image of unused pure Fe sample.

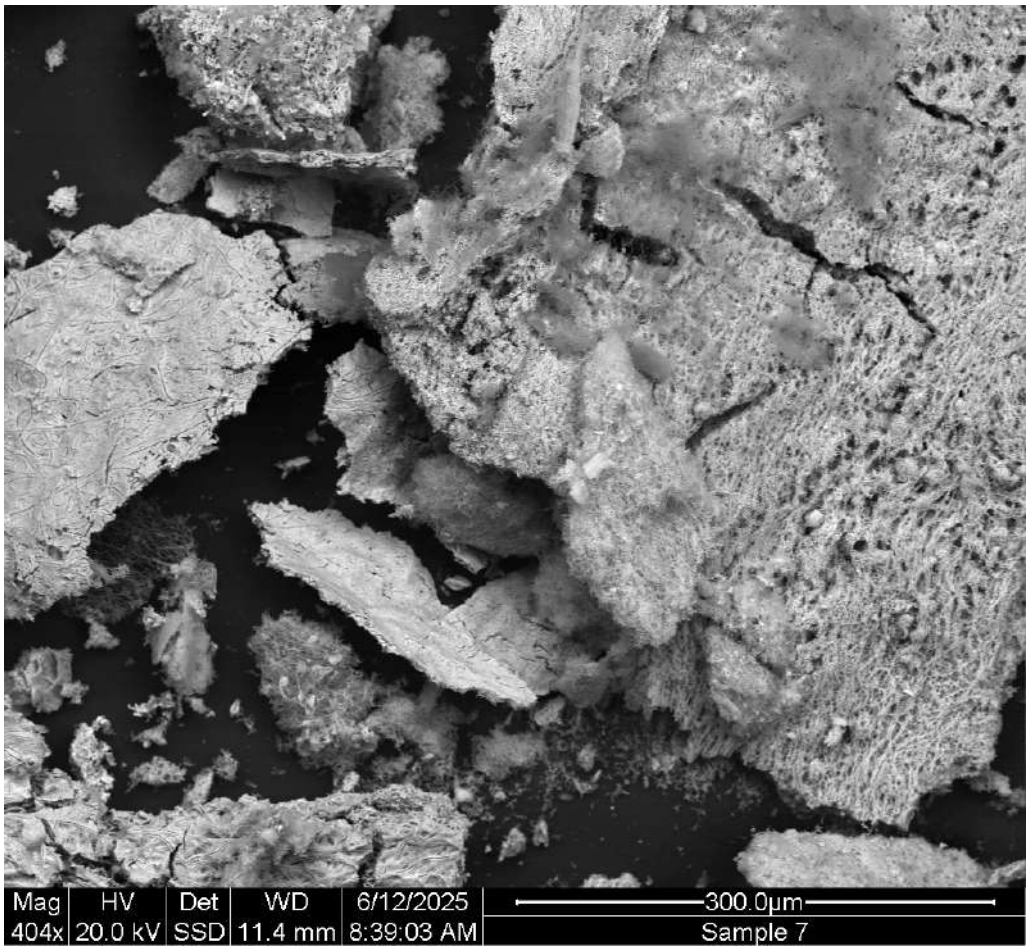

Figure A.3: SEM image of unused Fe-Sr sample. In the left side of the image there is some material which has lost its fibrous structure due to excessive metal loading.

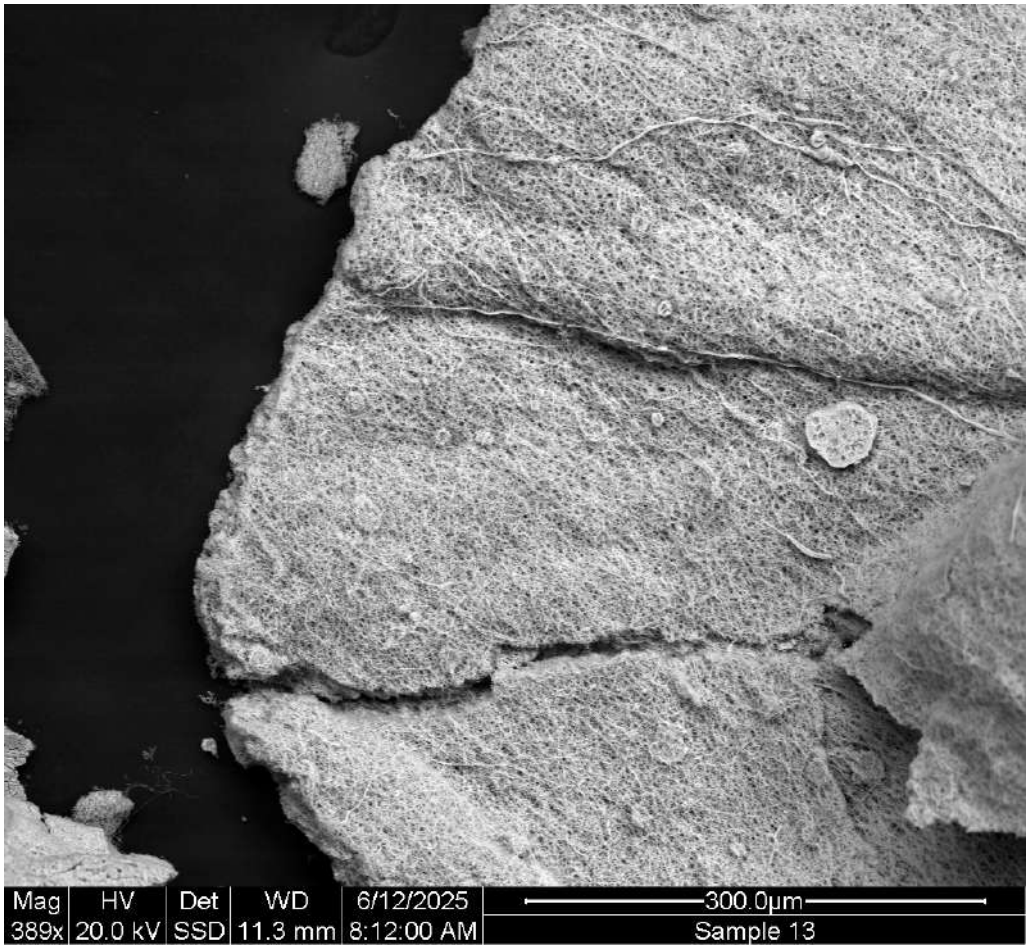

Figure A.4: SEM image of unused Fe-Ni sample.

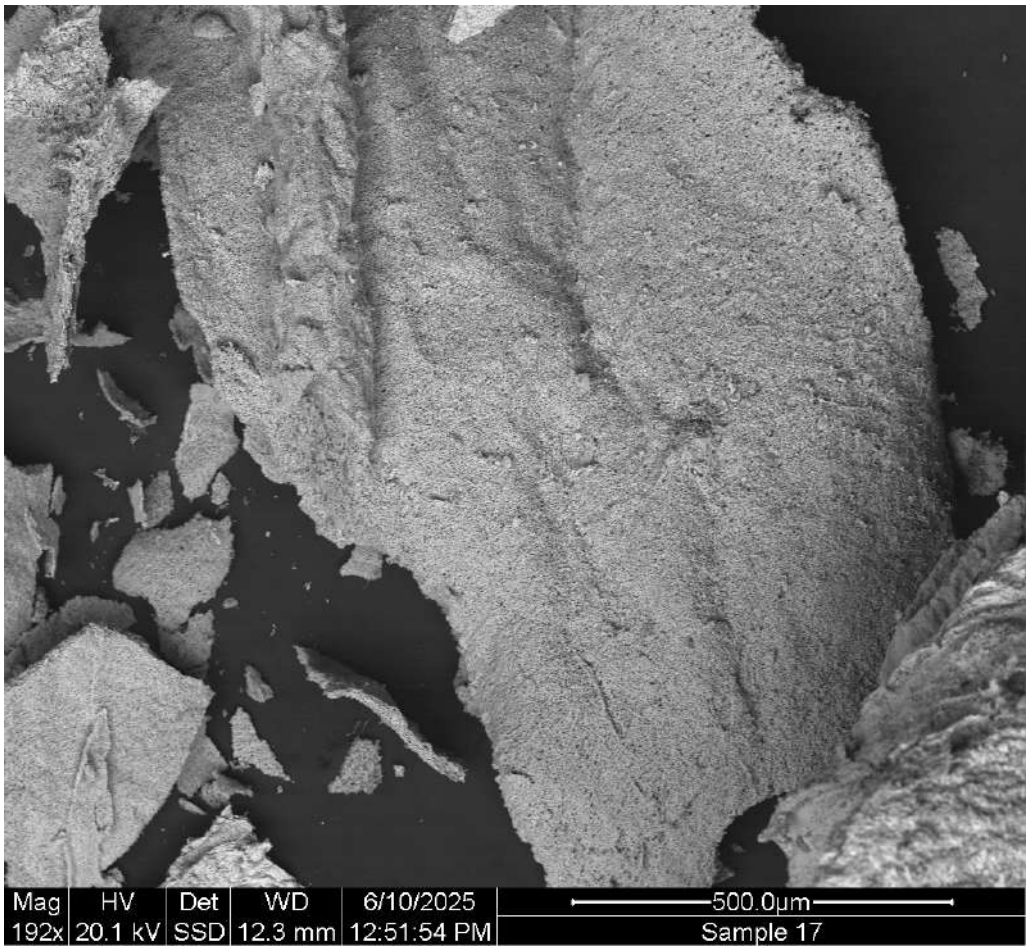

Figure A.5: SEM image of used pure Fe sample. The carbon deposition has not been removed from this sample.

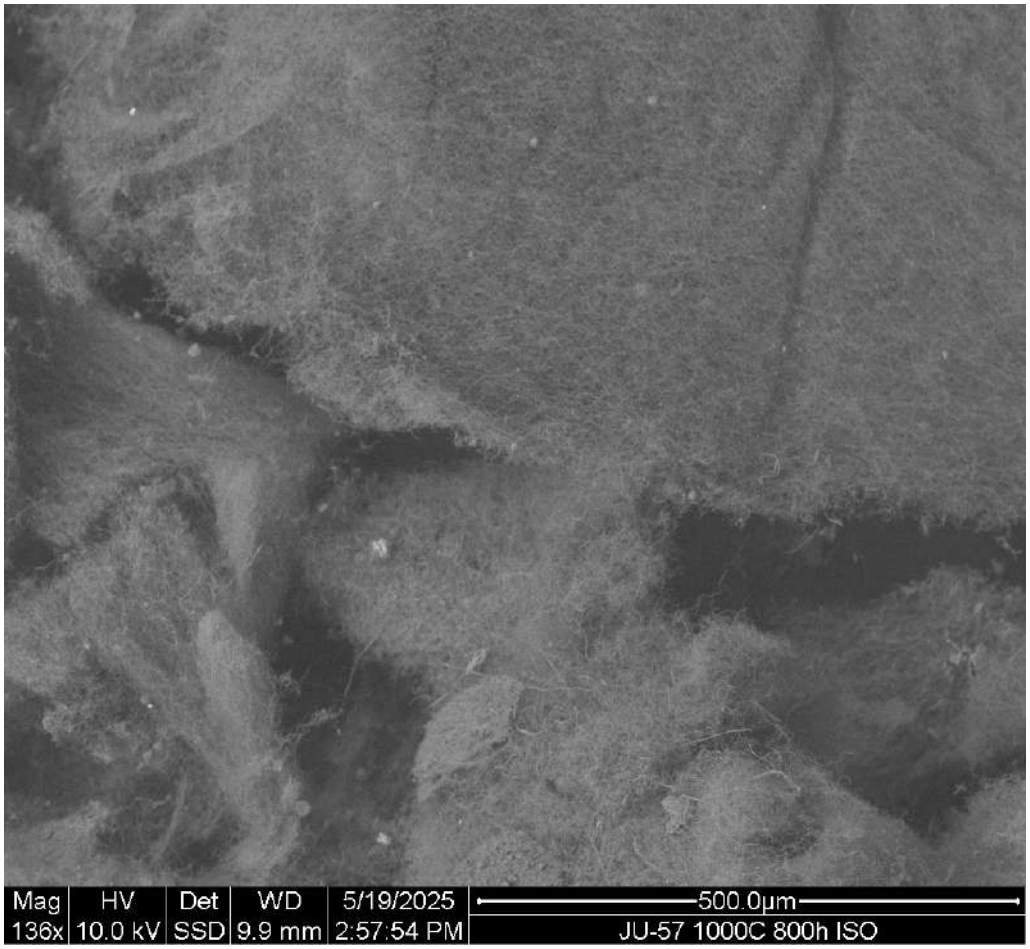

Figure A.6: SEM image of used and decarbonized alumina sample.

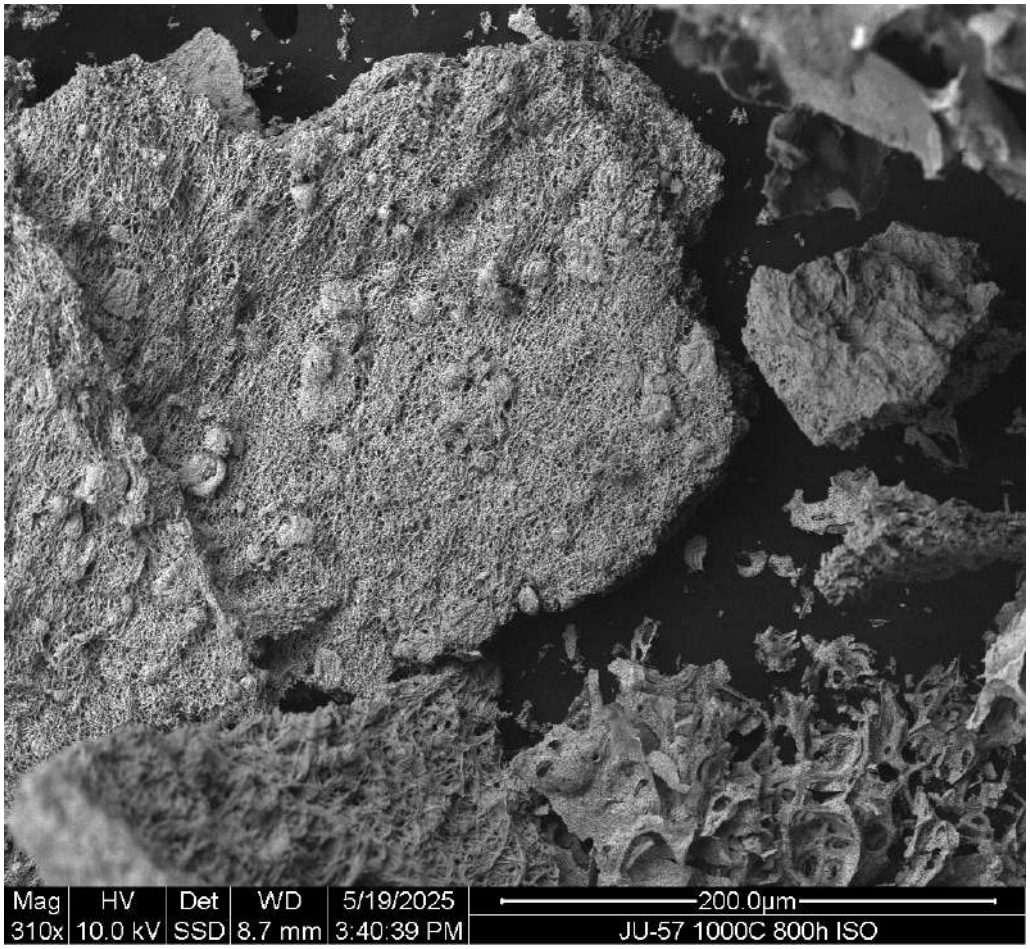

Figure A.7: SEM image of used and decarbonized Fe-Ce sample.

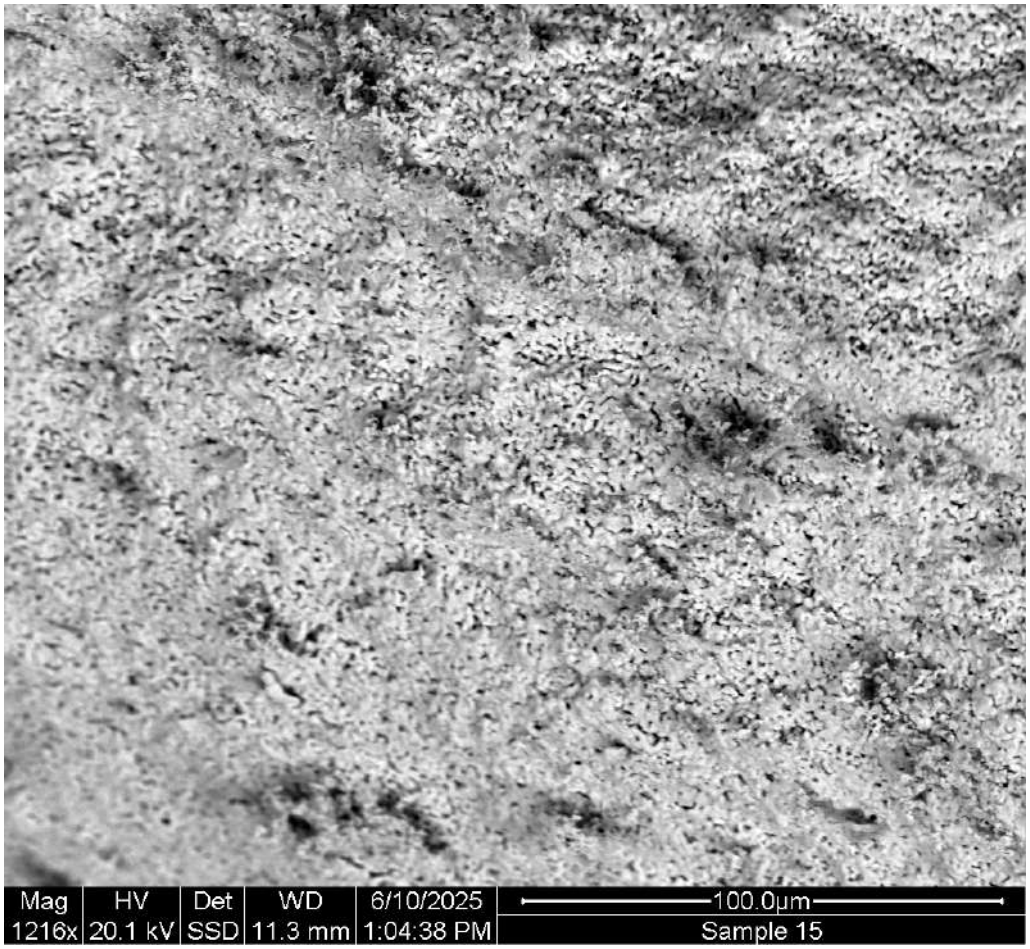

Figure A.8: SEM image of used and decarbonized Fe-Ni sample.

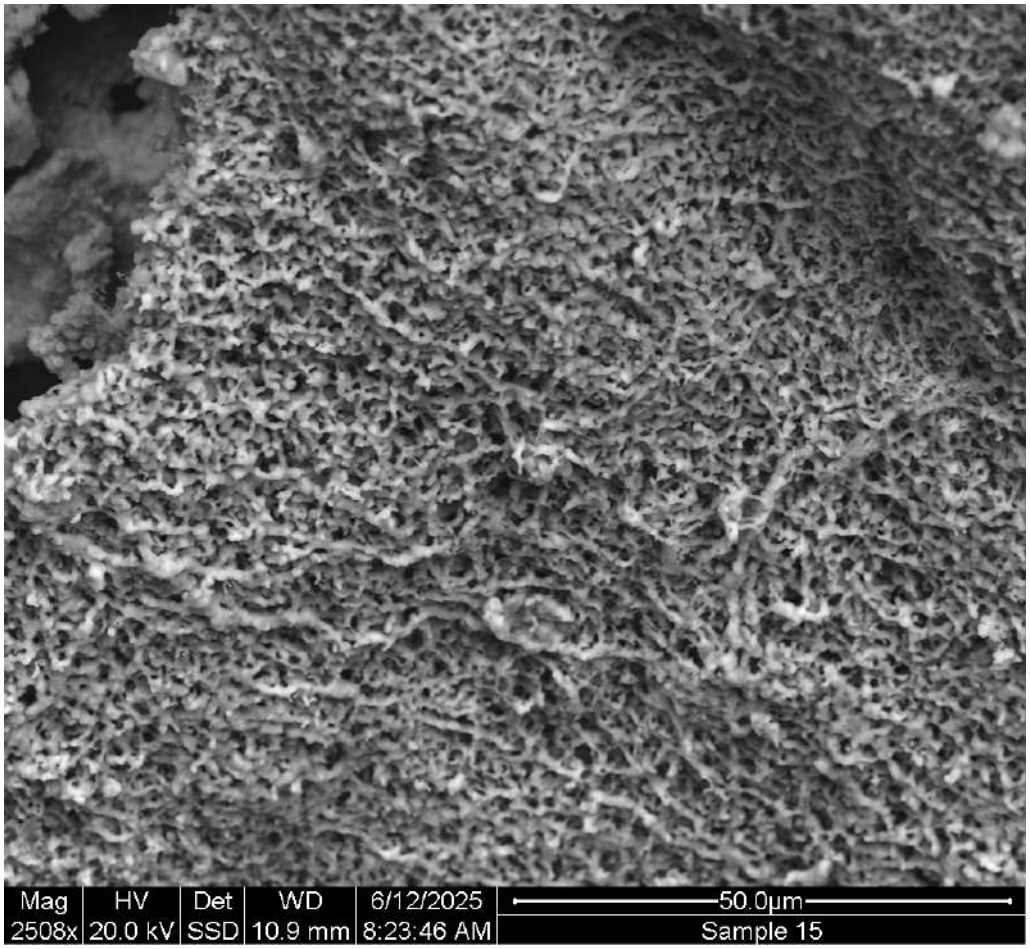

Figure A.9: SEM image of used and decarbonized FeNi sample

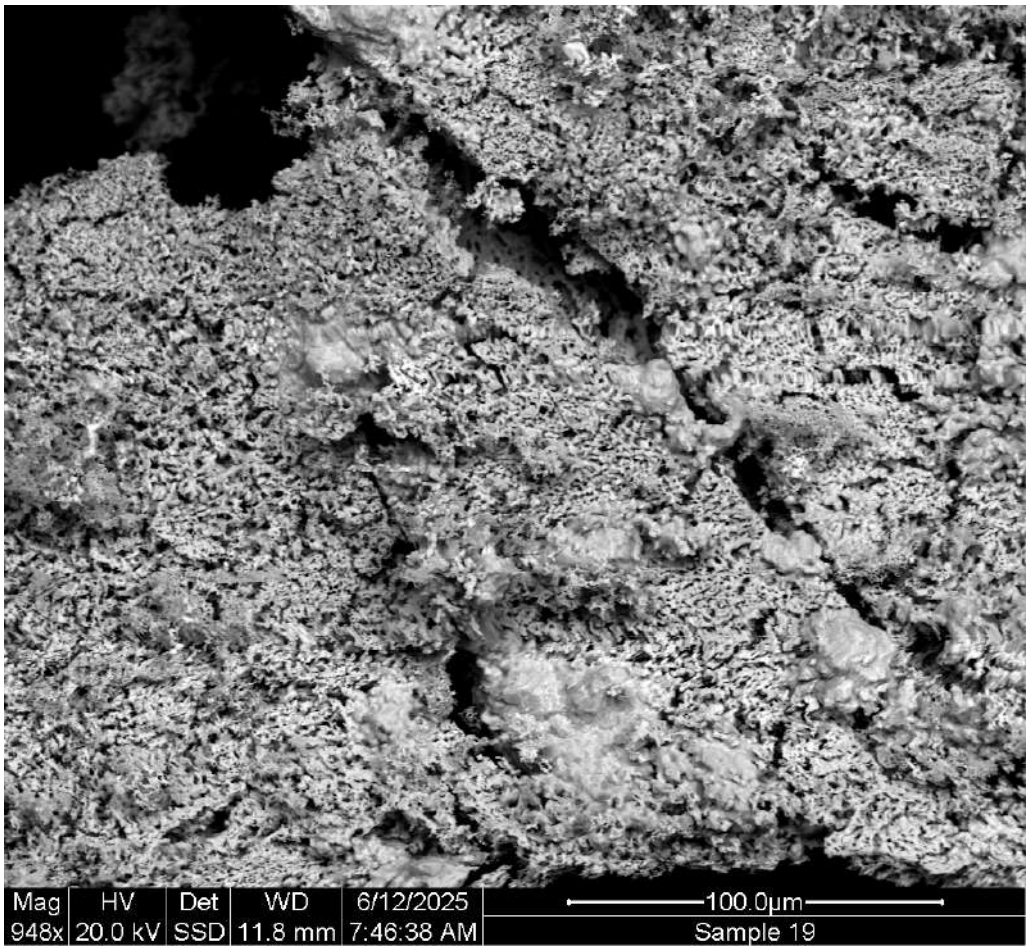

Figure A.10: SEM image of used and decarbonized Fe-Sr sample that was used in further testing and long cycle experiments.

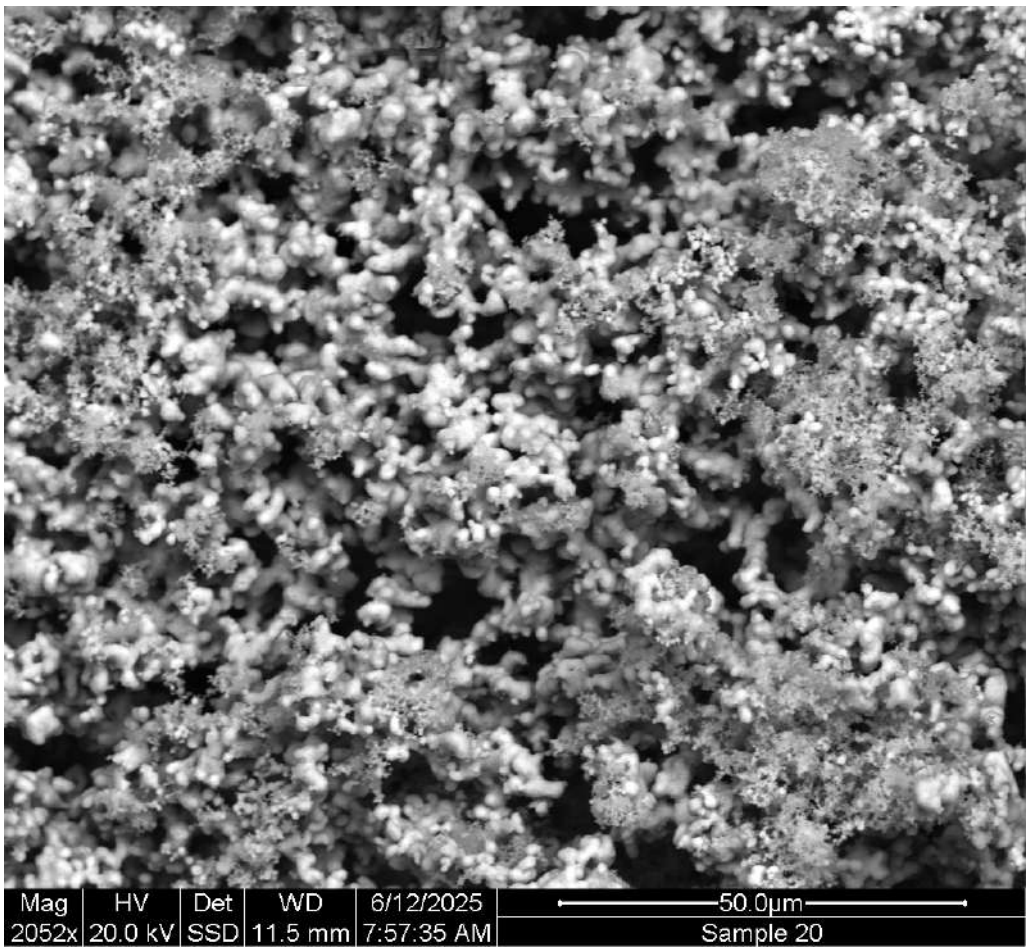

Figure A.11: SEM image of used and decarbonized Fe-Ni sample that was used in further testing and long cycle experiments. Some very fine fibrous structures can be seen among the more bulky fibrous structure.

Department of Chemistry and Chemical Engineering
CHALMERS UNIVERSITY OF TECHNOLOGY
Gothenburg, Sweden
www.chalmers.se

CHALMERS